University of Nevada, Reno

Developing a watershed modeling approach for reconstructing past streamflow in the upper Walker River Basin, California

A thesis submitted in partial fulfillment of the
requirements for the degree of Master of Science in
Environmental Science

By

Jasmine C. Vittori

Dr. Laurel Saito/Thesis Advisor

August, 2011

THE GRADUATE SCHOOL

We recommend that the thesis
prepared under our supervision by

JASMINE CHIANTI VITTORI

entitled

Developing A Watershed Modeling Approach For Reconstructing Past Streamflow In The Upper Walker River Basin, California

be accepted in partial fulfillment of the
requirements for the degree of

MASTER OF SCIENCE

Laurel Saito, Ph.D., P.E., Advisor

Franco Biondi, Ph.D., Committee Member

Douglas Boyle, Ph.D., Graduate School Representative

Marsha H. Read, Ph. D., Associate Dean, Graduate School

August, 2011

ABSTRACT

Measured streamflow data in a given basin are important for determining regional patterns of climate and streamflow trends, but are often unavailable or extend back less than 100 years. Observed streamflows can be regressed against tree-ring data that serve as proxies for streamflow to extend the measured record, however this empirical approach cannot account for factors that do not directly affect tree-ring growth, but which may influence streamflow. To reconstruct past streamflows in a more mechanistic way, seasonal water balance models were reviewed and developed for the upper West Walker River basin that can use proxy precipitation and air temperature data derived from tree-ring records. The final model incorporates simplistic relationships between temperature, precipitation, and other components of the hydrologic cycle, and operates at a seasonal time scale. The model was able to reproduce streamflow with an r^2 of 0.90, and a RMSE of 7.50 cm with average seasonal air temperature as input. Simulated streamflow was 0.66% greater than observed streamflow for WY 1940 through WY 2006. This model was subsequently used to simulate the effects of wildfire on streamflow in the upper West Walker River Basin. The earliest historical record of wildfire in this basin dates back to 1961, with the most recent recorded in 2005. Evapotranspiration and runoff coefficients were adjusted to simulate reduced vegetation cover as a result of fire, and were applied to the dry season when fire was recorded and the subsequent wet season to reflect time required for re-vegetation to occur. The resulting r^2 value decreased to 0.85, with RMSE increasing to 9.02 cm, and the overall streamflow simulation increased to 1.57% greater

than observed streamflow. Based on the results of this modeling exercise, the modeling approach with average seasonal air temperature would be appropriate for utilizing proxy tree-ring data as input. The model performed very well using only air temperature and precipitation as input and incorporated 6 parameters representing hydrologic processes influencing streamflow. However, simulating wildfire with this model did not improve streamflow simulations, indicating that the model was sensitive to modeling such landcover manipulations.

ACKNOWLEDGEMENTS

I would like to thank my committee members Dr. Laurel Saito, Dr. Franco Biondi, and Dr. Douglas Boyle for their help and support throughout this project. I would also like to thank Scotty Strachan, University of Nevada, Reno, for his help teaching the fieldwork sampling and analysis portion of this project. This material is based upon work supported by the National Science Foundation under Grant No. ATM-0823480.

TABLE OF CONTENTS

Abstract i

Acknowledgements iii

List of Tables v

List of Figures vi

Chapter 1: Introduction 1
Water Resources in the west..... 1
Extending instrumental records..... 3
Research goals 5
Water balance models..... 5
Previous work..... 7
Layout of thesis..... 12

Chapter 2: Methods 13
Study overview 13
Site description 13
Model selection and considerations 18
Model input & output 26
Parameter estimation 27
Assessment of best model for use with proxy data 32
"What-if" wildfire scenario 33

Chapter 3: Results & Discussion 35
Model error and uncertainty 35
Model performance 36
Assessment of best model for use with proxy data 49
"What-if" wildfire scenario 50

Chapter 4: Conclusions 55

References 57

Appendix 64

LIST OF TABLES

Table 1: Models investigated for use with tree-ring proxy data for seasonal streamflow reconstruction 20

Table 2: Acceptable ranges for parameter estimation, where *a* is the fraction of snowmelt and rain that becomes runoff; *b* is the fraction of infiltration that becomes ET; *c* is the fraction of GW that becomes baseflow; *d* is the fraction of GW that becomes GW flow; *e* is the temperature above which precipitation is rain; *f* is the temperature below which precipitation is snow, *s* is the temperature below which precipitation is snow; *w* is the temperature above which snow begins to melt, and *m* is meltmax. Constraints were set so that parameters $c + d \leq 1.0$; $s - w \geq 0.2$ (^{o}C); and $e - f \geq 0.2$ (^{o}C) 30

Table 3: Results of Monte Carlo simulations using PRISM data for input. Values shown are average ± one standard deviation, with ranges of values over the 500 simulations in parentheses. "*n"*= number of seasons modeled; "Std" means standard deviation 42

Table 4: Summary of model results using parameter values averaged over 500 Monte Carlo simulations for Models A and B with all temperature schemes. Values in bold represent the best outcome of the metric over all models 44

Table 5: Statistical measures for wildfire simulation compared to Model A_{ave} results 52

Table 6: Observed, Model A_{ave} simulated, and Wildfire simulated streamflow (cm/season) for the dry season when wildfire occurred and wet season immediately following 53

LIST OF FIGURES

Figure 1: Simple water balance model as modified by Saito et al. (2008). *a* is the fraction of precipitation that becomes runoff; *b* is the fraction of infiltration that evapotranspires; *c* is the fraction of groundwater (GW) storage that becomes baseflow; *d* is the fraction of GW storage that becomes GW flow; GW storage is the groundwater left after baseflow and GW flow are removed 8

Figure 2: Solander et al. (2010) temperature-index water balance model, where *a* is the fraction of snowmelt and rain that becomes runoff; *b* is the fraction of infiltration that becomes evapotranspiration; *c* is the fraction of GW storage that becomes baseflow; *d* is the fraction of GW storage that becomes GW flow; C_m = melt rate factor (cm $^oC^{-1}$ $month^{-1}$); T_b is the base temperature of snowpack (^oC); $T_{maxsnow}$ is the maximum temperature at which precipitation is snow (^oC) 10

Figure 3: Thornthwaite water balance model (McCabe and Markstrom 2007), where *r* is drofac, the fraction of rain that becomes direct runoff; *sr* is the runoff factor, a fraction of soil-moisture storage that becomes surplus runoff; *t* is STC, soil water storage capacity; *m* is meltmax, the maximum snowmelt rate applied to snow storage; *e* is the temperature above which all precipitation is rain (^oC); *f* is the temperature below which all precipitation is snow (^oC). PET is defined as potential ET; AET is defined as actual ET. This model also incorporates a parameter value for latitude that is not represented in the schematic 11

Figure 4: Walker River basin. The upper West Walker River basin is delineated in blue, with the entire Walker River Basin outlined in black 17

Figure 5: Model A; simple water balance model with WASMOD snow component, where *a* is the fraction of snowmelt and rain that becomes runoff; *b* is the fraction of infiltration that becomes ET; *c* is the fraction of GW that becomes baseflow; *d* is the fraction of GW that becomes GW flow; *s* is the temperature below which precipitation is snow; *w* is the temperature above which snow begins to melt. GW storage is the groundwater left after baseflow and GW flow are removed 23

Figure 6: Model B; simple water balance model with Thornthwaite snow component, where *a* is the fraction of snowmelt and rain that becomes runoff; *b* is the fraction of infiltration that becomes ET; *c* is the fraction of GW that becomes baseflow; *d* is the fraction of GW that becomes GW flow; *e* is the temperature above which precipitation is rain; *f* is the temperature below which precipitation is snow, and *m* is meltmax, the maximum melt rate. GW storage is the groundwater left after baseflow and GW flow are removed 25

Figure 7. Results of parameter estimation process for Model A and Model B using all temperature schemes for parameters *a*, *b*, *c*, and *d* 41

Figure 8. Results of parameter estimation process for Model B using all temperature schemes for parameters *e*, *f* and *m* 43

Figure 9. Results of parameter estimation process for Model A using all temperature schemes for parameters *s* and *w* 43

Figure 10: Model A_{ave}, the simple water balance model with WASMOD snow calculations incorporating average seasonal temperatures 45

Figure 11: Model A_{max}, the simple water balance model with WASMOD snow calculations incorporating maximum seasonal temperatures 45

Figure 12: Model A_{min}, the simple water balance model with WASMOD snow calculations incorporating minimum seasonal temperatures 46

Figure 13: Model $B_{ave,}$ the simple water balance model with Thornthwaite snow calculations incorporating average seasonal temperatures 47

Figure 14: Model B_{max}, the simple water balance model with Thornthwaite snow calculations incorporating maximum seasonal temperatures 48

Figure 15: Model B_{min}, the simple water balance model with Thornthwaite snow calculations incorporating minimum seasonal temperatures 48

Figure 16: Wildfires in the upper West Walker River basin between WY 1940 and 2006 50

Figure 17: Simulated streamflow incorporating wildfire effects compared to observed streamflow for the period between 1960 and 2006. No wildfire was recorded in this basin prior to 1961 51

Figure 18: Model A_{ave} initial *a*, *b*, *c* and *d* parameter values over 500 runs plotted against RMSE 67

Figure 19: Model A_{ave} initial *s* and *w* parameter values over 500 runs plotted against RMSE 68

Figure 20: Model B_{ave} initial *a*, *b*, *c* and *d* parameter values over 500 runs plotted against RMSE 69

Figure 21: Model B_{ave} initial *e*, *f* and *m* parameter values over 500 runs plotted against RMSE 70

Figure 22: Model A_{ave} initial *a*, *b*, *c* and *d* parameter values over 500 runs plotted against r^2 71

Figure 23: Model A_{ave} initial *s* and *w* parameter values over 500 runs plotted against r^2 72

Figure 24: Model B_{ave} initial *a*, *b*, *c* and *d* parameter values over 500 runs plotted against r^2 73

Figure 25: Model B_{ave} initial *e*, *f* and *m* parameter values over 500 runs plotted against r^2 74

Figure 26: Model A_{ave} initial *a*, *b*, *c* and *d* parameter values over 500 runs plotted against %bias 75

Figure 27: Model A_{ave} initial *s* and *w* parameter values over 500 runs plotted against %bias 76

Figure 28: Model B_{ave} initial *a*, *b*, *c* and *d* parameter values over 500 runs plotted against %bias 77

Figure 29: Model B_{ave} initial *e*, *f* and *m* parameter values over 500 runs plotted against %bias 78

CHAPTER 1: INTRODUCTION

Water resources in the west

Water resource variability is of particular importance in the arid western United States where water resources are already limited and population is rapidly growing (Brockerhoff 2000). Increasing development and population are expected to further increase the demand for water resources in this region (Horton 1996). Infrastructure consisting of expensive aqueducts and reservoirs has been developed in many areas in the western U.S. to supply water to urban areas from distant sources (Hundley 1992). Methods such as this may be needed more in the future to meet continued and increasing demands.

In addition, water supplies in the western states are anticipated to decrease due to increased demand and as a result of climate change. According to current trends and future projections outlined by Seager et al. (2007) and Field et al. (2007), precipitation patterns and temperatures in the western U.S. have already been changing and are projected to continue. In mountainous regions that receive precipitation in the form of snow, air temperature increases have changed timing and frequency of precipitation events, resulting in an increase in precipitation in the form of rain rather than snow, and differences in when precipitation falls in the season and when snow melts (Stewart et al. 2004, Field et al. 2007, Maurer et al. 2007, Day 2009). A decrease of approximately 15-30% in snow water equivalent during spring, and decrease in snow cover in the

mountainous west during spring and summer over the last 50+ years has been observed (Field et al. 2007). This trend in temperature is projected to continue, thus continuing to impact spring/summer snowmelt as well as growing seasons and number of frost-free days. These changes have implications for influencing streamflow, which has been increasing in the eastern part of the U.S. but decreasing in the western states (Field et al. 2007, Sharpe et al. 2007, Sheppard 2010), with peak streamflow in western mountain ranges occurring 1-4 weeks earlier than in the 1940's (Stewart et al. 2004, Field et al. 2007). The changes in timing of snowmelt have been correlated with wildfire frequencies (Westerling et al. 2006), which can in turn impact streamflow by reducing evapotranspiration (ET) (Wohlegemuth et al. 2006) and causing an increase in surface runoff (Beyers et al. 2005, Wohlegemuth et al. 2006). An overall "drying" of the southwestern U.S. is projected (Seager et al. 2007). There are indications that more frequent and severe droughts have already been occurring in the west (Field et al. 2007).

Current climate models predict average annual air temperatures will increase to levels ranging 1-2 ^{o}C higher than today by 2050 in the western U.S. which could affect water availability by influencing changes in precipitation type and snowmelt. As the demand for water resources increases, it is important to understand how water resource availability will change. This is particularly important in the western U.S. where water is already a limited resource, and availability can be severely influenced by climate and climate change. One of the challenges for understanding the impacts of climate change on water availability is understanding past trends and the implications for future trends. Instrumental climate data are limited to approximately 100 years or so, providing only a

brief snapshot of past climate for that period of time. Measured streamflow data typically span 100 years at most as well, which is not long enough to determine long-term responses to climate change (Saito et al. 2008, Gray and McCabe 2010, Solander et al. 2010), and there is need to extend streamflow records in a way that will allow a better understanding of the past.

Extending instrumental records

Dendrochronology using moisture sensitive tree species can greatly improve our understanding of past climate and streamflow where observational data are limited (Swetnam et al. 1999, Hurteau et al. 2007, Sheppard 2010). Tree-rings have been used to reconstruct a number of climatic variables related to the hydrology of a given area including streamflow, snowpack, and drought (Woodhouse 2003, Woodhouse et al. 2009). Thus, analyses using dendrochronology can provide proxy data for measured data that are limited or nonexistent. Other sources of proxy data can include pollen records, ice cores, and sediment cores, but the use of tree-rings is much better at producing climatic records at finer temporal resolutions, such as annual or seasonal time series of precipitation variability or air temperature (Biondi et al. 2005, Sheppard 2010). Variations in ring sequence width signify changes in rates of tree growth, which is a function of nutrient availability, location, climatic variables, and tree species, and the degree to which tree-rings can represent climatic variability can be greatly influenced by many factors including the species of tree and surrounding environment (Biondi 1999, Hurteau et al. 2007).

Traditionally, streamflow reconstructions using tree-rings have been generated using regression approaches that extend records back hundreds or thousands of years, providing the ability to examine past trends. Correlation between tree-ring growth and climate factors such as precipitation can be regressed against measured precipitation values to generate a much longer climate record (Campelo et al. 2009). However, these approaches do not incorporate physical processes impacting streamflow such as evapotranspiration and infiltration, and how these processes may be affected by changes in land-use patterns, geomorphology or vegetation dynamics (Saito et al. 2008, Solander et al. 2010). Problems with regression-based streamflow reconstructions from tree-ring data can arise in cases such as with wildfire. The higher runoff, lower infiltration, and lower evapotranspiration due to decreased vegetation after wildfire (Wohlegemuth et al. 2006) could result in a higher streamflow than what a streamflow reconstruction derived from tree-rings would indicate if based solely on regression techniques.

Tree-ring data can also be used as proxy input data for more mechanistic, physical process-based reconstructions, such as through the use of a watershed model (Saito et al. 2008, Gray and McCabe 2010, Solander et al. 2010). Watershed models allow for investigation of the influence of physical processes such as infiltration, evapotranspiration, snowmelt, or runoff on streamflow (Saito et al. 2008, Solander et al. 2010), which regression-based streamflow reconstructions cannot do. The use of tree-ring records with a watershed model can allow for better understanding of the variability of streamflow reconstructions and their sensitivity to situations such as wildfire.

Research goals

This research project consisted of investigation and further development of a method for incorporating tree-ring proxy precipitation and air temperature data with a seasonal water balance model to reconstruct past streamflow in the upper Walker River Basin, CA, USA. The ultimate goal of this research is to utilize a mechanistic modeling approach to reconstruct past streamflow, and to investigate how climate-independent factors such as changes in land cover or infiltration could influence estimates of past flows, something regression-based models are not able to do. Methods such as this can provide useful information about interactions of various components of the water cycle, including the interaction between runoff, snowmelt, and evapotranspiration under warmer climatic regimes.

Water balance models

Water balance models were first developed decades ago, and have been revised over time for many different uses (Alley 1984, Xu 2002). These models have been used for water management issues such as determining seasonal patterns of irrigation demand, soil moisture stresses, and prediction of streamflow. Water balance models keep track of water input and outflow by accounting for precipitation and snowmelt, evapotranspiration, streamflow, runoff and groundwater (Alley 1984). Water balance models range from extremely simplistic to very complex, depending on what is represented and what the model objectives are.

Simple water balance models incorporate mechanisms impacting streamflow such as evapotranspiration, infiltration, groundwater flow, and runoff and generally have few parameters (Xu and Singh 1998). They have been used to investigate hydrologic cycles on many different spatial and temporal scales. Most commonly they have been used on a daily time scale, but they have been increasingly used at monthly as well as yearly temporal resolutions, especially when used for climate-related research and projections (Xu and Singh 1998). The water year (WY), defined as the 12-month period beginning October 1st through September 30th of the following year, is considered a closed annual water budget in northern latitudes because all snow typically melts during spring/summer and therefore does not carry over to the following WY. Because of this, it may not be necessary to model snow at the annual WY time scale in western U.S. watersheds. Modeling snow is, however, an important factor for investigation of seasonal snowmelt influences on hydrologic processes because some snow will carry over into the next time step.

Runoff due to snowmelt from mountainous catchments is an important source of water in the western United States. The quantity and timing of the runoff depend on a number of interdependent factors that relate to climate, vegetation, and topography (Kelleners et al. 2010). Snowmelt alone accounts for more than 80% of streamflow in California (Maidment 1993) and has also been cited as a primary source of groundwater recharge, runoff, and soil moisture in the arid/semi-arid western U.S. (Maidment 1993, Marks et al. 1999, Kelleners et al. 2010). Thus, modeling snowmelt is crucial for

modeling water resources in arid regions dependent on water supplies derived from snowpack.

Unfortunately in many regions, modeling snow faces the same problems modeling streamflow does: limited instrumental data. Some basins have instrumentation for measuring snow depth, though this is measured primarily in valleys, and many basins have no instrumentation at all (Stanzel et al. 2008). Extrapolation of air temperature, precipitation, wind speed, cloud cover, albedo, and many other factors that influence snow and snowmelt can be difficult, and can be significantly different across short distances (Ferguson 1999). There are many approaches for modeling snowmelt, including the temperature-index or degree-day approaches, which are frequently-used empirical methods for estimating snowmelt, and the energy balance method (Walter et al. 2005), which uses short-wave and long-wave radiation to calculate snowmelt and typically requires more input data.

Previous work

Several studies have been done thus far relating tree-ring patterns to hydrologic modeling at a watershed scale. These models investigated the use of either precipitation as the only input, or both precipitation and air temperature input to model the hydrologic processes for surface runoff, ET, groundwater flow, baseflow, and snowmelt (Saito et al. 2008, Gray and McCabe 2010, Solander et al. 2010).

Saito et al. (2008) used a water balance model adapted from a model developed by Fiering (1967) to model the upper West Walker River watershed in California. This

simple watershed model operated on a WY timescale and represented observed data reasonably well (r^2 = 0.87, n = 63 years), but did not include a snow component (Saito et al. 2008). Without snow the Saito et al. (2008) model has four parameters (Figure 1).

Figure 1. Simple water balance model as modified by Saito et al. (2008). *a* is the fraction of precipitation that becomes runoff; *b* is the fraction of infiltration that evapotranspires; *c* is the fraction of groundwater (GW) storage that becomes baseflow; *d* is the fraction of GW storage that becomes GW flow; GW storage is the groundwater left after baseflow and GW flow are removed.

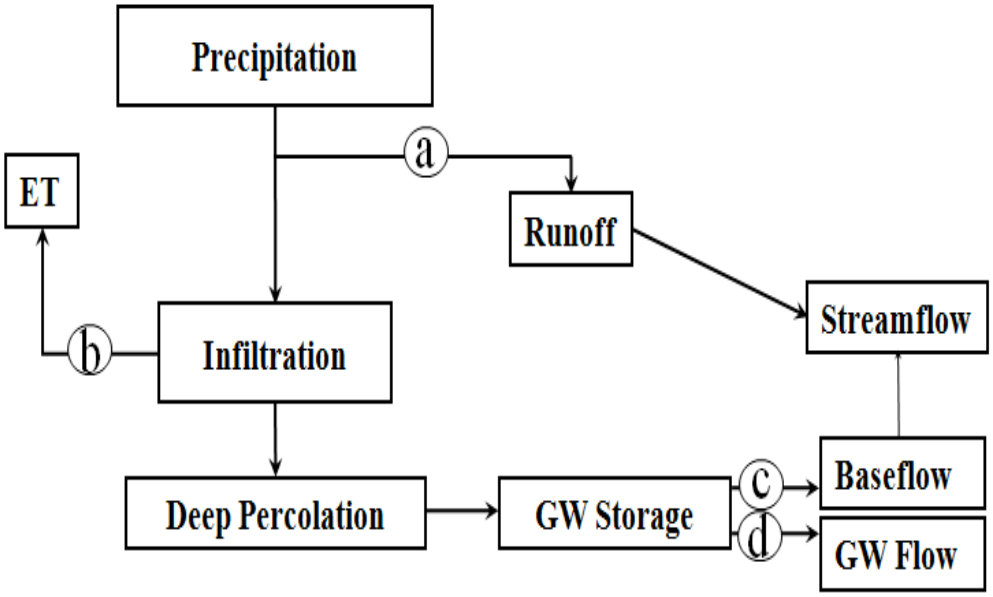

Solander et al. (2010) modified the model used by Saito et al. (2008) to operate on a seasonal timescale and used a temperature-index approach for addressing snow precipitation and melt to incorporate the influence of snow on hydrologic processes. The simplicity of the temperature-index approach for modeling snow precipitation and melt has led to its wide use for ice and snowmelt calculations in modeling (Hock 2003, Walter

et al. 2005). This model was calibrated to the upper Meadow Valley Wash watershed in southeastern Nevada, and comparison of calibrated model output to observed data had an r^2 of 0.81 (n = 18 years). However, some calibrated parameter values were unrealistic and end-of-May snow was not accounted for. This particular basin had the added complications of a dam and upstream diversions for seasonal irrigation, which both influence streamflow during part of the year. Thus, this model was only used for the part of the year with natural flow regimes when such diversions were not supposed to occur. Figure 2 shows the setup of the Solander et al. (2010) model.

Gray and McCabe (2010) utilized the monthly Thornthwaite water balance model (McCabe and Markstrom 2007) to generate annual streamflows for the Upper Yellowstone drainage. Model calibration resulted in an r^2 of 0.71 for the period of 1911 to 1995 using the Parameter-Elevation Regressions on Independent Slopes Model (PRISM) precipitation and air temperature data as input. PRISM estimates precipitation and temperature values for regions with no instrumentation by using spatial datasets, point data, and digital elevation models (Daly et al. 1994). When PRISM temperature data and tree-ring-derived precipitation were used as input, model calibration resulted in an r^2 of 0.56. Tree-ring derived precipitation data were developed at an annual resolution by calibrating tree growth against PRISM precipitation for the record between 1895 and 2004 (Daly et al. 1994).

Figure 2. Solander et al. (2010) temperature-index water balance model, where *a* is the fraction of snowmelt and rain that becomes runoff; *b* is the fraction of infiltration that becomes evapotranspiration; *c* is the fraction of GW storage that becomes baseflow; *d* is the fraction of GW storage that becomes GW flow; C_m = melt rate factor (cm $^{o}C^{-1}$ $month^{-1}$); T_b is the base temperature of snowpack (^{o}C); $T_{maxsnow}$ is the maximum temperature at which precipitation is snow (^{o}C).

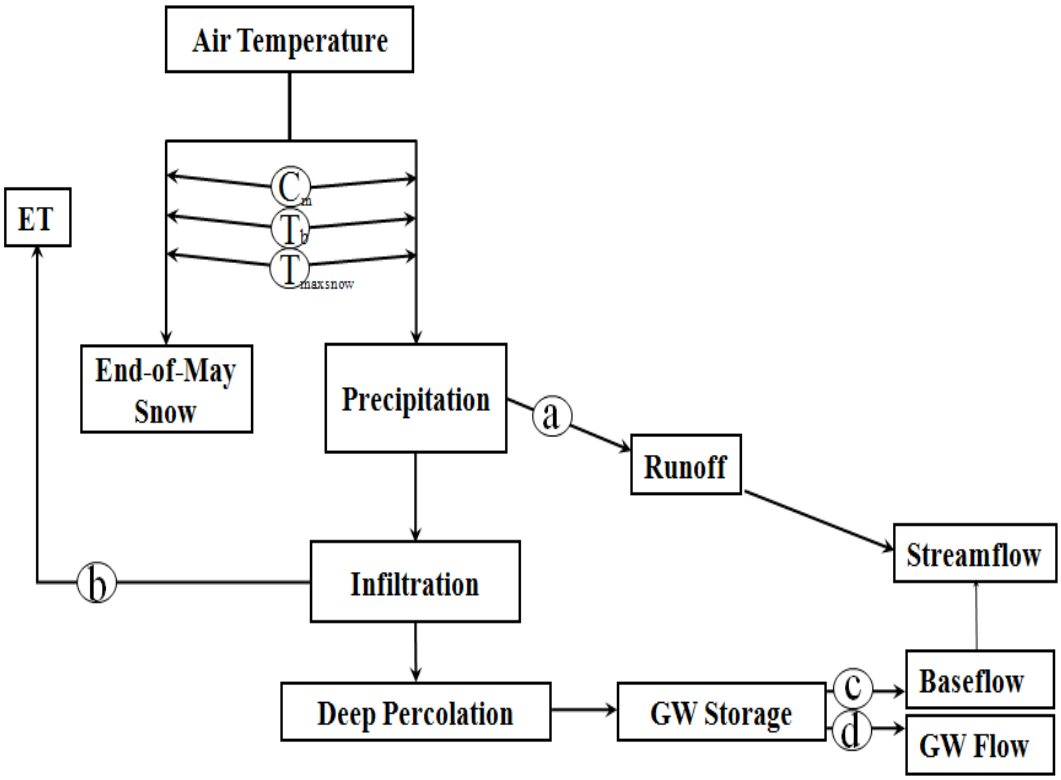

The Thornthwaite water balance model has been in use for decades (Thornthwaite 1948, McCabe and Markstrom 2007), requires only precipitation and air temperature input, and incorporates a snow component. The model uses 7 parameters to account for snow precipitation, rain precipitation, latitude, soil water storage capacity, direct runoff, surplus runoff, and snowmelt and operates on a monthly time step. To model the Upper Yellowstone drainage at an annual resolution, Gray and McCabe (2010) performed a

series of aggregation and disaggregation steps, which can introduce more uncertainty into the modeling process. Figure 3 depicts how the Thornthwaite model is set up (McCabe and Markstrom 2007).

Figure 3. Thornthwaite water balance model (McCabe and Markstrom 2007), where *r* is drofac, the fraction of rain that becomes direct runoff; *sr* is the runoff factor, a fraction of soil-moisture storage that becomes surplus runoff; *t* is STC, soil water storage capacity (cm); *m* is meltmax, the maximum snowmelt rate applied to snow storage; *e* is the temperature above which all precipitation is rain (°C); *f* is the temperature below which all precipitation is snow (°C). PET is defined as potential ET; AET is defined as actual ET. This model also incorporates a parameter value for latitude that is not represented in the schematic.

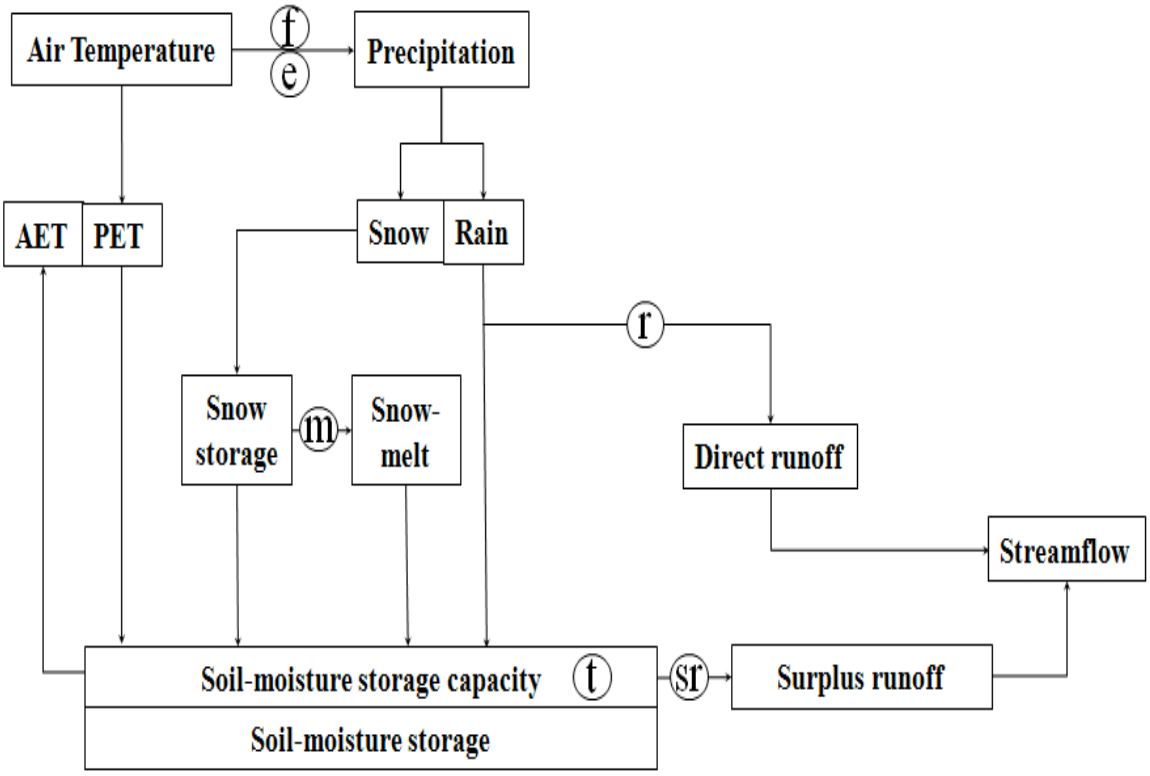

Layout of thesis

This thesis is organized in chapters, with the first chapter providing a background of water balance models, previous research relating to this project, and the importance of understanding past climate as it relates to water resources variability. The second chapter provides details of the study methods including justification for model structure, the model set-up and boundary conditions, and descriptions of how data were organized and analyzed. Results of the modeling approaches were outlined and discussed in the third chapter, with discussion focused on the various models' results based on criterion outlined in the methods. The final chapter discusses the conclusions of this research.

CHAPTER 2: METHODS

Study Overview

This study began with an investigation and review of water balance models that would be suitable for use with proxy tree-ring climate records for reconstructing seasonal streamflow in the upper West Walker River at the USGS streamflow gauge (gauge number 10296000) near Coleville, CA. Once suitable models were determined, modifications were incorporated into each model to allow modeling at a seasonal time step and account for snow precipitation and melt. Due to the temporal resolution of tree-ring data, a smaller time step is not possible. The models were then run in a parameter estimation process to determine performance statistics for each model and to determine the "best" model to subsequently use for wildfire scenario modeling. Results from the wildfire scenario were examined to assess model sensitivity to such occurrences.

Site description

The Walker River watershed originates in the eastern Sierra Nevada mountain range near Bridgeport, CA, crossing over the California border into Nevada, and terminating at Walker Lake, NV, approximately 250 kilometers downstream. Headwaters of the Walker River originate at elevations greater than 3,000 meters and the entire watershed includes more than 10,600 km^2 along the western boundary of the Great Basin (Sharpe et al. 2007). The majority of streamflow in the river originates as snowmelt from the Sierra Nevada snowpack. This snowpack provides water storage for surrounding and downstream irrigated agriculture, recreation, fisheries, habitat, and municipal uses.

During a typical year, river volume increases as snow melts during spring, with peak flow usually occurring in May or June. During years with deep snowpack in winter, however, peak flow can occur as late as July. During years with little snowpack, flow can be severely decreased and remain low throughout the rest of the year (Sharpe et al. 2007). This can have dramatic impacts on those who depend on the downstream flow. A large research project in the Walker River watershed is currently investigating water conservation, economic impacts, and river channel health and issues (Sharpe et al. 2007).

Climate in the upper Walker River Basin varies seasonally, with cold winters and precipitation in the form of snow, and dry hot summers. This basin is on the eastern side of the Sierra Nevada mountain range within a rain shadow, which drastically reduces the amount of precipitation received on eastern slopes. Precipitation falls primarily in the form of snow, but when rain does occur, flooding can result from rainfall melting snow at higher elevations (rain-on-snow events), altering streamflow in the Walker River (Sharpe et al. 2007). Average annual precipitation measured in the nearest town to the upper Walker River basin, Bridgeport, CA, is 2.54 cm. Temperatures can vary greatly in this region, ranging from an average minimum temperature of -4.4 ^{o}C in winter to an average maximum temperature of 16.7 ^{o}C in summer as measured at Bridgeport, CA (WRCC 2006).

The geology of the Walker River Basin centers around the modern Sierra Nevada batholiths, which formed around 225 to 65 million years ago (Hill 1975). These batholiths formed as molten granitic material that invaded the sedimentary rock below the surface of the earth (Hill 1975). Magma melted existing rock, partially incorporating

some of it, and depositing veins of gold and other metals. The intense heat from the molten granitic material caused new minerals to crystallize in overlying volcanic and sedimentary rock, creating metamorphic rock in the process (Hill 1975). Once buried, the molten material cooled over several million years before solidifying into large bodies of granite. These bodies of granite now form the modern Sierra Nevada mountain range. During this time, natural environmental chemical processes, or "weathering," were eroding the overlying external rock, exposing the batholiths in the region until finally becoming an area of low, gently rolling granitic hills.

Around 20 million years ago volcanic eruptions blanketed the area with lava flows and volcanic material (Reed 1933). As eruptions increased in frequency, the eastern edge of the modern Sierra Nevada mountain range began to rise and tilt along fault lines. These processes of uplift and erosion continue to shape and wear down the Sierra Nevada mountain range (Hill 1975). The eastern side of the range is considerably more tilted at approximately 25^{o} and is less weathered due in part to the rain shadow on this side of the range (Reed 1933). The oldest known rocks in the Sierra Nevada consist of limestone, chert, shale, and sandstone, much of which has been modified by metamorphic processes into schist, marble, slate, and quartzite. The fossils that have been found date back to Paleozoic, Triassic, and Jurassic periods (Reed 1933, Hill 1975).

Humans began to occupy the area at least 11,000 years ago (Wilkinson 1992, Grayson 1993, Horton 1996). As with many other watersheds in the west, there has been and continues to be a considerable demand on water resources in this region for fish, agriculture, development, and mining (Wilkinson 1992, Horton 1996). Explorer Peter

Ogden discovered the Walker River sometime around 1829, though few records from this event exist. Continued exploration of the region utilized the river as a "guide" across the Sierra Nevada. Once settlers began migrating westward in search of gold, settlement near water sources began in earnest, and the west fork of the Walker River was utilized as a water source for herdsman and ranchers who settled in Smith Valley and Mason Valley between 1856 and 1859 (Horton 1996).

While only approximately 25% of the Walker River watershed lies in California, most of the precipitation that contributes to streamflow in the watershed falls within that 25%. The majority of water consumption in the watershed lies downstream in both California and Nevada. Uses for irrigation around Topaz Lake, in Antelope Valley, Smith Valley, and Mason Valley account for almost 90% of the water consumption in the basin (Horton 1996). Further downstream uses include habitat creation and maintenance at the Mason Valley Wildlife Management Area (Sharpe et al. 2007, NDOW 2010), cooling ponds for NVenergy's Fort Churchill Power Generating Station (NVenergy 2010), and recreational uses along the river and at Walker Lake, where the river terminates. This study focuses in the upper West Walker River, a sub-basin of the Walker River basin near the headwaters of the west fork of the Walker River (Figure 4).

Figure 4. Walker River basin. The upper West Walker River basin is delineated in blue, with the entire Walker River Basin outlined in black.

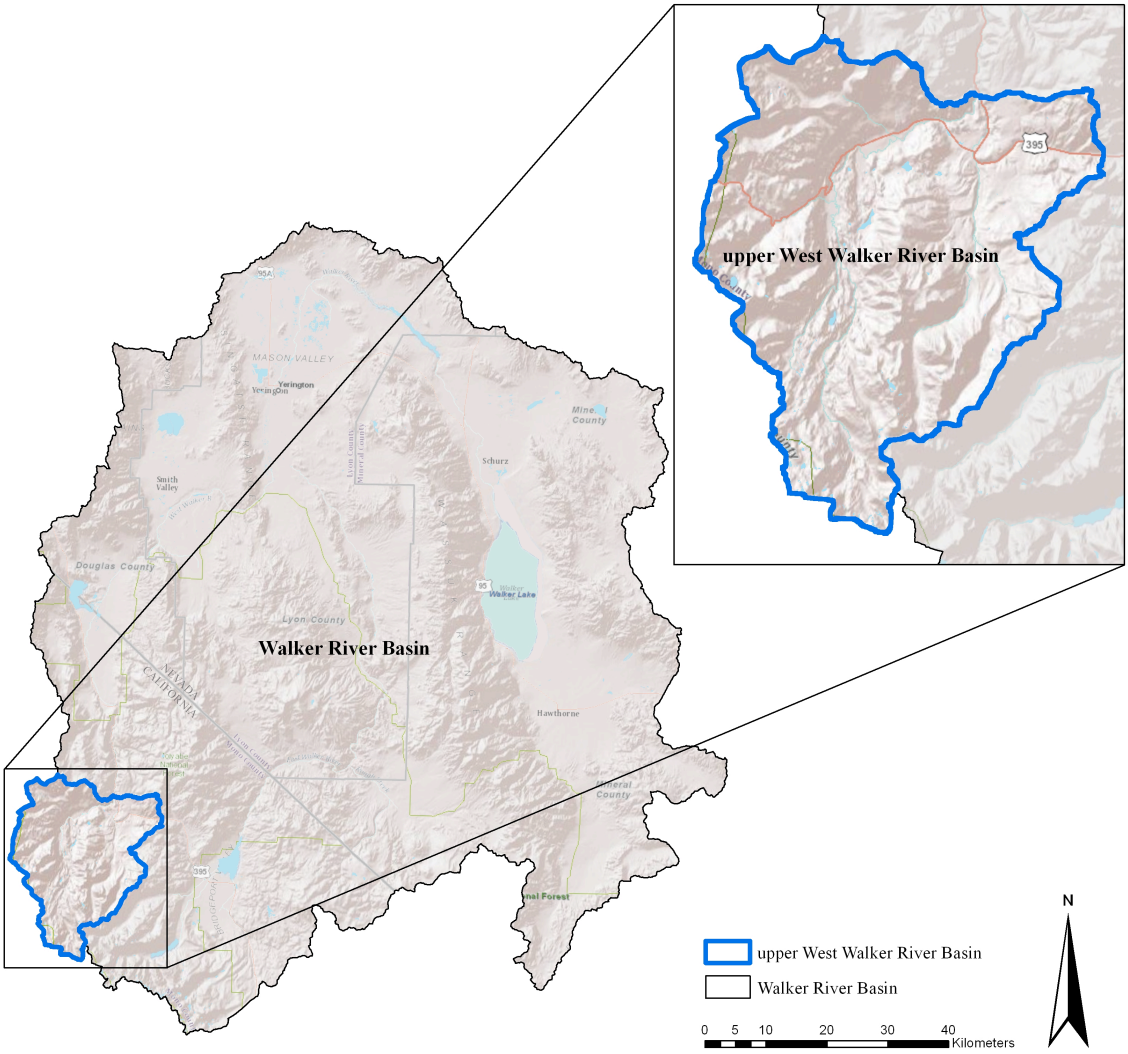

The upper West Walker River basin is characterized by high elevations with minimal development that includes areas for camping, fishing, and a small Marine Corps Mountain Warfare Training Facility. This region has not been directly utilized for

agricultural crops and thus does not have diversions or dams influencing streamflow. Wildfires have been recorded periodically in the upper West Walker River, with 7 occurring in 1991 alone. The most recent fire to occur in the region was in 2005.

Model selection and considerations

There are a number of important considerations in selecting a water balance model for reconstructing streamflow using tree-ring proxy data. Firstly it is widely recognized that many watershed models require a significant amount of input data (Farmer et al. 2003). Tree-ring records can only produce proxy precipitation and air temperature data, so reconstructing streamflow using proxy data from tree-ring records requires a model that only needs air temperature and precipitation data as input. The lack of available data indicates that the model structure should be simplistic to reduce introduced error (Atkinson et al. 2002, Farmer et al. 2003, Butts et al. 2004). Another consideration for choosing a simplistic water balance model is that increasing model structure complexity may lead to over-parameterization.

Secondly, the upper Walker River basin is dominated by snow precipitation, as are many other basins in the western U.S. Because snowmelt contributes heavily to streamflow in this basin, it is important to model snowmelt changes and the effect on streamflow regimes. Using a simple water balance model approach can allow the flexibility to incorporate a snow modeling component while maintaining a simple model structure.

Thirdly, reconstructing streamflow using tree-ring proxy data is limited to modeling at an annual or possibly seasonal temporal resolution. Patterns of tree-ring growth cannot be easily analyzed at finer temporal resolutions (Sheppard 2010). Models operating at time scales finer than annual or seasonal will require disaggregation that will introduce more uncertainty into the modeling approach. For this study, models were set up at a seasonal resolution to better represent snowmelt and precipitation.

Several water balance models were evaluated for their suitability for reconstructing seasonal streamflow based on data and model limitations. Models such as TOPMODEL (Beven 1997) and SEAMOD (Salas and Cardenas 1989) incorporate topography, soil characteristics, basin storage and ET, but were deemed inappropriate for use in this project because they need more input, introduce too many parameters, work at too fine of a timescale, and/or do not incorporate a snow component (Table 1).

The WASMOD model (Water And Snow balance Model) approach for factoring snow precipitation and melt (Xu 2002) has promise for use with proxy tree-ring air temperature data, though the full WASMOD model introduces too many parameters and requires too many inputs to be a viable model for streamflow reconstruction. The Thornthwaite modeling approach (McCabe and Markstrom 2007) is another potential model that could be used, as it too incorporates a simplistic way to account for snow, while having few parameters and requiring only air temperature and precipitation input. However, ET was only dependant on temperature inputs, so it would not be changed by altered land cover. In addition, the Thornthwaite model operates at a monthly time step and would require aggregation or model modification to operate at longer time steps.

Table 1. Models investigated for use with tree-ring proxy data for seasonal streamflow reconstruction.

MODELS	Snow component	No. of parameters	Timescale	Disadvantages
TOPMODEL (Beven 1997)	YES	5	Hourly	Not seasonal
Seasonal Model (SEAMOD) (Salas and Cardenas 1989)	NO	7 Without snow	Seasonal	No snow, Too many parameters
Water And Snow balance Model (WASMOD) (Xu 2002)	YES	3-6	Weekly Monthly	Need humidity Not seasonal
Simple Water Balance Model (Saito et al. 2008)	NO	4 Without snow	Annual	No snow Not seasonal
Water Balance Model with Temperature Index (Solander et al. 2010)	YES	7	Seasonal	Was not run for both seasons, Requires further development
Thornthwaite Water Balance Model (McCabe and Markstrom 2007)	YES	7	Monthly Annual	Not seasonal

The simple water balance model adapted from Fiering (1967) by Saito et al. (2008) was examined, but it does not have a snow component and operates at an annual timescale. Although the Solander et al. (2010) model was seasonal and included a snow

component, it was only used to model the wet season. Ultimately, models were narrowed down to the simple water balance used by Saito et al. (2008) that was augmented with WASMOD snow calculations (Model A), and the simple water balance model used by Saito et al. (2008) that was augmented with the Thornthwaite water balance model snow calculations (Model B). These models were chosen because they met the required criteria, or were easily modified to meet the necessary requirements. Both models were set up for seasonal 6 month time steps running from the beginning of the WY in October through March (wet season), and from April to the end of the WY in September (dry season).

The simple water balance model used by Saito et al. (2008) (Figure 1) uses equations 1-8:

Eq. 1 $SR_t = a * P_t$, $0 \le a \le 0.9$

Eq. 2 $ET_t = b * I_t$, $0 \le b \le 1$

Eq. 3 $BF_t = c * GS_{t-1}$, $0 \le c \le 1$

Eq. 4 $GF_t = d * GS_{t-1}$, $0 \le d \le 1$, $0 \le c + d \le 1$

Eq. 5 $I_t = P_t - SR_t$

Eq. 6 $DP_t = I_t * ET_t$

Eq. 7 $GS_t = GS_{t-1} + DP_t - BF_t - GF_t$

Eq. 8 $Q_t = SR_t + BF_t$

where SR_t = surface runoff for season t; ET_t = evapotranspiration for season t; BF_t = baseflow for season t; GF_t = groundwater flow for season t; I_t = infiltration for season t; DP_t = deep percolation for season t; GS_t = groundwater storage for season t; GS_{t-1} = groundwater storage for previous season (or initial boundary condition for season 1); P_t = precipitation for season t; and Q_t = streamflow for season t.

For Model A, two additional parameters determine how much precipitation is snow, and how much of that snow melts during the each season using equations 9-12:

Eq. 9 $$snow_t = P_t \left\{ 1 - e^{[(c_t - s)/(s-w)]^2} \right\}^+$$

Eq. 10 $$melt_t = sp_{t-1} \left\{ 1 - e^{-[(c_t - w)/(s-w)]^2} \right\}^+$$

Eq. 11 $$rain_t = P_t - snow_t$$

Eq. 12 $$sp_t = sp_{t-1} + snow_t - melt_t$$

where the plus sign (+) means $x^+ = \max(x,0)$ (Xu 2002), P_t is defined as precipitation at season t, c_t is air temperature (^oC) for season t, *s* is temperature below which precipitation is snow (^oC), and *w* is temperature above which all snow begins to melt (^oC). $Snow_t$ is defined as snow during season t, $rain_t$ is the amount of precipitation that was rain during season t (Eq. 11) for surface runoff determination, and sp_t is defined as the snowpack during season t (Eq. 12). The simplicity of the WASMOD snow component in Model A allows the use of air temperature to estimate snowmelt and runoff from determinations of how much precipitation falls in the form of snow, and at which temperature the snow

melts. In this model melt is directly calculated based on temperature, rather than from a separate melt factor. Figure 5 depicts how Model A is set up.

Figure 5. Model A; simple water balance model with WASMOD snow component, where *a* is the fraction of snowmelt and rain that becomes runoff; *b* is the fraction of infiltration that becomes ET; *c* is the fraction of GW that becomes baseflow; *d* is the fraction of GW that becomes GW flow; *s* is the temperature below which precipitation is snow; *w* is the temperature above which snow begins to melt. GW storage is the groundwater left after baseflow and GW flow are removed.

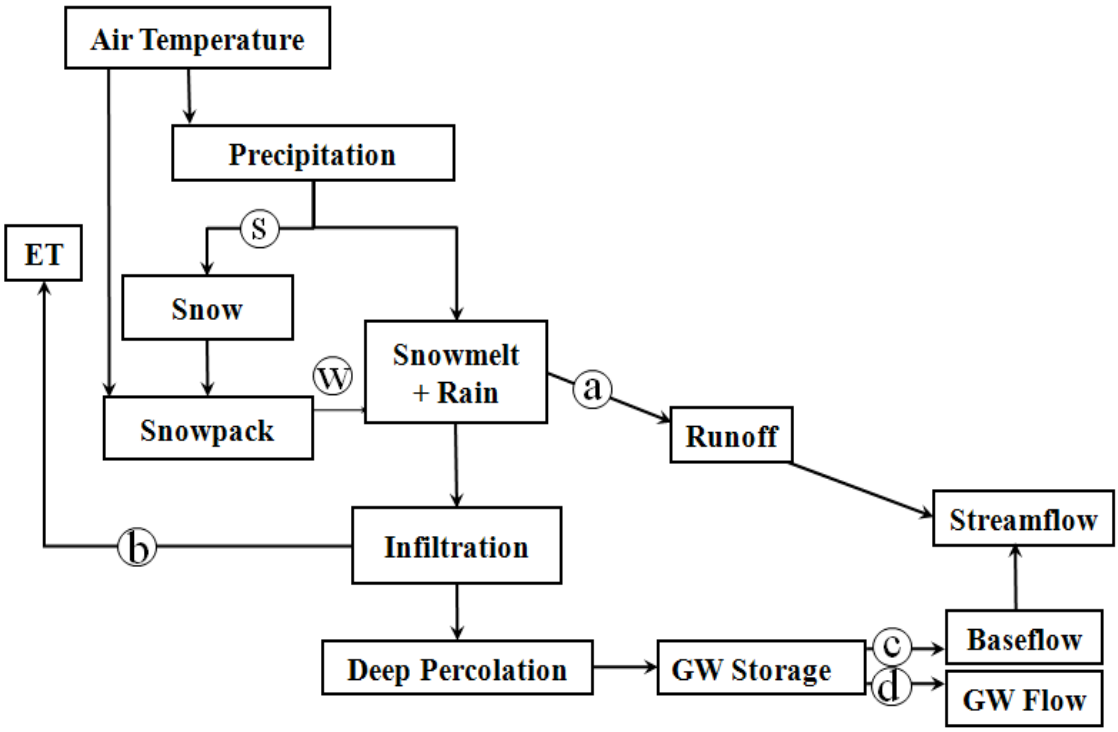

Model B operates at the same seasonal scale as Model A and also requires only precipitation and air temperature input. The original Thornthwaite water balance model uses 7 parameters to account for snow precipitation, rain precipitation, latitude, soil water

storage capacity, direct runoff, surplus runoff, and snowmelt, and operates at a monthly time step (McCabe and Markstrom 2007). In this adaptation of the Saito et al. (2008) model the snow component has parameters for temperature above which all precipitation is rain (*e*), temperature below which all precipitation is snow (*f*), and a fraction representing the maximum snowmelt rate, *m* (meltmax). T_t is the temperature at season t. Snow precipitation (P_{snow}) falling between the thresholds for *e* and *f*, and rain precipitation (P_{rain}) are calculated based upon these three parameters in Equations 13 and 14, respectively.

Eq. 13 $$P_{snow} = P * \left[\frac{e - T_t}{e - f} \right]$$

Eq. 14 $$P_{rain} = P - P_{snow}$$

When snow has been calculated, accumulation is determined through equations 15-16, taking into account snowmelt, storage, and the meltmax factor, *m*:

Eq. 15 $$SMF_t = m * \left[\frac{T_t - f}{e - f} \right]$$

Eq. 16 $$Melt_t = snostor - SMF$$

where SMF is the fraction of snow storage that melts during season t (cm); *m* is meltmax; T_t is the temperature (^oC) for season t; *f* is the temperature below which all precipitation is snow (^oC); *e* is the temperature above which all precipitation is rain (^oC); snostor is the amount of snow storage for season t (cm), and $Melt_t$ is snowmelt (cm) during season t that is added to rain precipitation to determine surface runoff. In the event that SMF is greater than *m*, SMF is set to meltmax. Figure 6 depicts how Model B is set up. Equations for both Model A and Model B were entered into Microsoft Excel to run the models.

Figure 6. Model B; simple water balance model with Thornthwaite snow component, where *a* is the fraction of snowmelt and rain that becomes runoff; *b* is the fraction of infiltration that becomes ET; *c* is the fraction of GW that becomes baseflow; *d* is the fraction of GW that becomes GW flow; *e* is the temperature above which precipitation is rain; *f* is the temperature below which precipitation is snow, and *m* is meltmax, the maximum melt rate. GW storage is the groundwater left after baseflow and GW flow are removed.

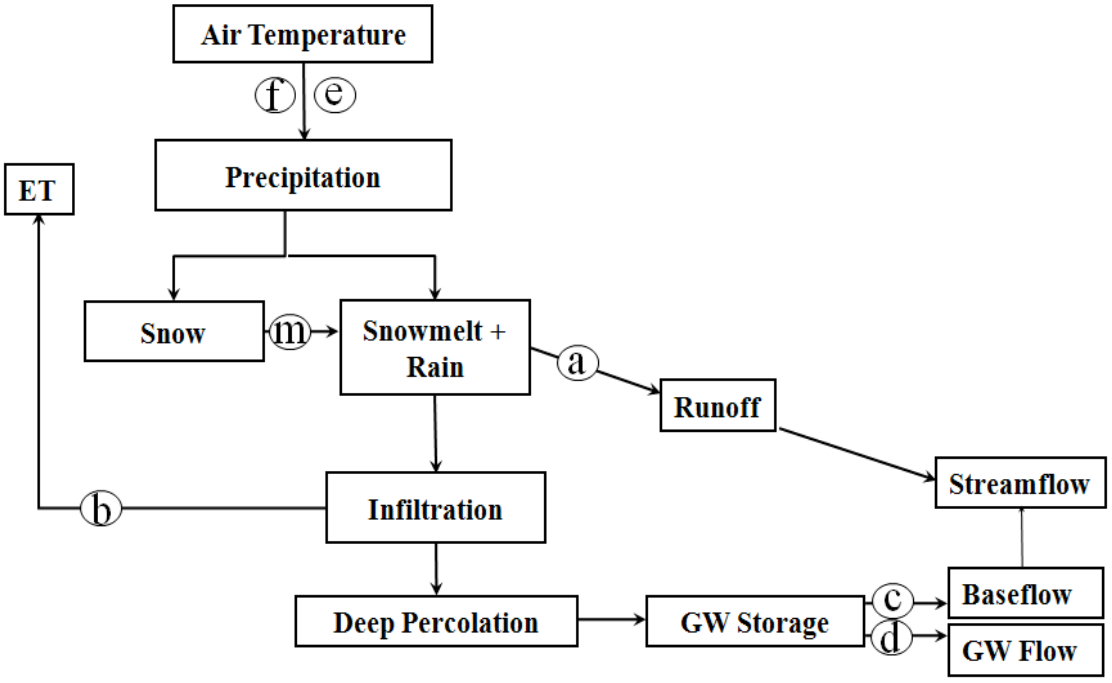

Model input & output

PRISM air temperature and precipitation values for WY 1940-2006 were used in lieu of proxy air temperature and precipitation data as input during model parameter estimation. PRISM data were obtained at 2.5 arc-minute resolution for 12 grids representing the upper West Walker River Basin that included the Coleville, CA USGS gage 10296000. These data are available at monthly time steps from the PRISM Climate Group (Daly et al. 2000). Because the resolution of temperature derived from tree-rings can only be seasonal at best, it was necessary to determine what temperatures to use to represent seasonal temperatures. Monthly maximum and minimum PRISM air temperatures were averaged for each month over all months of the season to get maximum and minimum seasonal temperatures representing each season. In addition, monthly maximum and minimum temperatures were averaged to get monthly average temperatures which were then averaged over the season to get average seasonal temperatures. Once temperature data were processed, they were incorporated into each model in order to determine how each model performed based on different temperature schemes. Model A incorporating minimum seasonal temperature is denoted "Model A_{min}," Model A incorporating maximum seasonal temperature is denoted "Model A_{max}," and Model A incorporating average seasonal temperature is denoted "Model A_{ave}." Similarly, "Model B_{min}," "Model B_{max}," and "Model B_{ave}" denote Model B incorporating minimum, maximum, and average seasonal temperatures, respectively.

Data processing was also done to aggregate monthly PRISM precipitation and observed streamflow to a seasonal time step. Both precipitation and streamflow were

summed over each wet and dry season. Output from model parameter estimation was streamflow discharge in cm/season. Measured streamflow during WY 1940–2006 at USGS gauge station 10296000, West Walker River near Coleville, CA, was used for comparison of modeled results. The water balance model was calibrated using 66 years of seasonal stream flow data from the USGS streamflow gauge. According to Vogel (2006), water balance models should be calibrated with at least 30 years of continuous data.

Parameter estimation

An important step in the model identification process is the estimation of a suitable parameter set that has feasible values and produces reasonable model outputs. Model parameters are usually estimated through calibration of measured time-series of runoff (streamflow discharge) over a sufficiently long period (Butts et al. 2004). The required length of the time-series depends, among other things, on the complexity of the model structure used and available data. It might range from a short period of time for a simple model structure to a long period of time for a more complex model. Regardless of model structure, it is important to calibrate a model using a sufficient length of time to avoid the problem of simulating a climate period that may not be representative of the regional climate as a whole (Wagener and Wheater 2006).

For this study, the parameters of each model structure were adjusted until the observed system output and the model output showed acceptable levels of agreement. Manual calibration does this in a trial-and-error procedure, often using a number of different measures of performance and visual inspection of plotted seasonal streamflow

(Boyle et al. 2000). It can yield good results, but can also be very time consuming (Wagener et al. 2003). Manual calibration also allows a degree of researcher subjectivity, which can lead to introduced error. Automated parameter estimation can reduce both time, and subjectivity. Thus, Excel "Solver" was used to estimate parameters that resulted in estimated streamflows that most closely matched observed streamflows at the Coleville, CA gage.

Model parameter estimation was conducted using a "Monte Carlo" style approach with uniform starting value distribution similar to the one used in Saito et al. (2008) and Solander et al. (2010). This style of approach is common and is used to determine if the same parameter results are returned when different, random starting parameter values are used (Wagener et al. 2003). It is particularly useful when there is a high level of uncertainty associated with acceptable parameter values, as well as when using a model that is underdetermined, and this method provides a more robust and reliable estimate of parameters (Wagener et al. 2003). The approach works by starting with random parameter values, finding "best" fit between simulated and observed streamflow, and repeating the process over multiple runs. For this study this process was run 500 times.

Model parameters for Model A included snow/rain temperature thresholds (s, w), the proportion of rain plus snowmelt that became surface runoff (a), the proportion of infiltration that was lost through evapotranspiration (b), the proportion of groundwater that became baseflow (c), and the proportion of infiltration that became groundwater flow (d). In addition, the initial groundwater storage (GS_i) needed to be estimated. Parameter estimation was done for these parameters for 66 years of the measured streamflow record

(WY 1940-2006). For Model B, the same parameters controlling surface runoff (*a*), the proportion of infiltration that was lost through evapotranspiration (*b*), the proportion of groundwater that became baseflow (*c*), and the proportion of infiltration that became groundwater flow (*d*) were adjusted as well as the snow components controlling snowmelt, (meltmax, *m*), rain precipitation (*e*), and snow precipitation (*f*).

To apply the Monte Carlo approach, random values were generated for initial parameter values within acceptable ranges (Table 2). These boundaries (ranges) were determined based on soil conditions in the upper West Walker River basin, availability of infiltrated water and GW storage, and current literature. The upper boundary for parameter *a* was set at 0.9 as in Saito et al. (2008) because soil survey data acquired from the National Resources Conservation Service for this area is classified as Soil Group D, indicative of slower infiltration rates and higher surface runoff. These soils consist primarily of clays that have a high shrink-swell potential, soils that have a clay pan or clay layer at or near the surface, and soils that are shallow over nearly impervious material, and/or soils that have high water table (NRCS 1993). These soils have a very slow rate of water transmission, therefore, the upper boundary for parameter *a* was set to reflect a higher runoff potential. The upper boundaries for *b*, *c*, and *d* were set to 1.0, as ET, baseflow, and GW flow could not exceed available infiltrated water or GW storage (Saito et al. 2008). Lower boundary conditions for *a*, *b*, *c*, and *d* were set to 0.0. Boundary conditions for the snow component in the models, temperature below which all precipitation was snow (*s*), temperature above which snow melted (*w*), temperature above with all precipitation was rain (*e*), temperature below which all precipitation was snow (*f*)

for Model B, and the maximum melt rate fraction, *m*, were based on Solander et al. (2010) and Gray and McCabe (2010), and ranged between 0.0 ^{o}C to 3.89 ^{o}C.

Table 2. Acceptable ranges for parameter estimation, where *a* is the fraction of snowmelt and rain that becomes runoff; *b* is the fraction of infiltration that becomes ET; *c* is the fraction of GW that becomes baseflow; *d* is the fraction of GW that becomes GW flow; *e* is the temperature above which precipitation is rain; *f* is the temperature below which precipitation is snow, *s* is the temperature below which precipitation is snow; *w* is the temperature above which snow begins to melt, and *m* is meltmax. Constraints were set so that parameters $c + d \leq 1.0$; $s - w \geq 0.2$ (^{o}C); and $e - f \geq 0.2$ (^{o}C).

Model A Parameters	Ranges	Model B Parameters	Ranges
a	$\geq 0.0; < 0.9$	*a*	$\geq 0.0; < 0.9$
b	$\geq 0.0; < 1.0$	*b*	$\geq 0.0; < 1.0$
c	$\geq 0.0; < 1.0$	*c*	$\geq 0.0; < 1.0$
d	$\geq 0.0; < 1.0$	*d*	$\geq 0.0; < 1.0$
s (^{o}C)	$\geq 0.0; \leq 3.89; > w$	*e* (^{o}C)	$\leq 3.89; > f$
w (^{o}C)	$\geq 0.0; \leq 3.89; < s$	*f* (^{o}C)	$\geq 0.0; < e$
		m	$> 0.0; < 1.0$

Once random values were entered, the Excel add-in Solver was used to iterate and minimize the root mean squared error (RMSE) for simulated versus observed streamflow according to Equation 15,

Eq. 15 $$RMSE = \sqrt{\frac{1}{n}\sum_{t=1}^{n}\left(Q_t^{sim} - Q_t^{obs}\right)^2}$$

where "*n*" is defined as the number of observations (in this case the number of seasons), and Q_t^{sim} and Q_t^{obs} are defined as the simulated and observed streamflow values (in centimeters per season) at time-step t, respectively. 500 sets of random initial parameter values were simulated in Excel. Solver ran through 100 iterations with each set of random initial parameter values to arrive at the lowest RMSE. In addition to RMSE, coefficient of determination (r^2) (Equation 16), and percent bias (Equation 17) were calculated to evaluate model performance:

Eq. 16 $$r^2 = \left(\frac{\sum_{t=1}^{n}\left(Q_t^{obs} - \overline{Q}^{obs}\right)\left(Q_t^{sim} - \overline{Q}^{sim}\right)}{\sqrt{\sum_{t=1}^{n}\left(Q_t^{obs} - \overline{Q}^{obs}\right)^2}\sqrt{\sum_{t=1}^{n}\left(Q_t^{sim} - \overline{Q}^{sim}\right)^2}} \right)^2$$

Eq. 17 $$\%Bias = \frac{\sum_{t=1}^{n}(Q_t^{sim} - Q_t^{obs})}{\sum_{t=1}^{n}Q_t^{obs}} \times 100$$

where $\overline{Q}_t^{sim}$ and $\overline{Q}_t^{obs}$ are defined as the averages of simulated and observed streamflow at time-step t, respectively. r^2 is commonly used to evaluate the representation of general trends of observed data, RMSE is commonly calculated to quantify the difference between observed and simulated data, and %bias is used to determine the overall under- and over- estimation of simulated estimates compared to observed data.

Assessment of best model for use with proxy data

Preliminary tree-ring streamflow reconstructions for the upper Walker River basin had an r^2 of 0.22 over the period between 1939 and 2001 (Saito et al. 2008), and have since been improved to an r^2 of 0.47 (unpublished results from F. Biondi). Improvement of proxy data from tree-rings can further improve regression-based streamflow reconstructions and improve both model function and performance, but was not in the scope of this research. Although proxy data could not be used as input to the model, statistical results from Model A and Model B were compared to determine which model was the best candidate for use with proxy tree-ring data. In addition, the models were evaluated regarding which temperature scheme used (maximum, minimum, or average seasonal temperature) provided the best results. Because future simulations with the selected model can only use one parameter set, parameters calculated by averaging the outcomes of the 500 Monte Carlo runs were used as input to generate and evaluate model statistics and performance.

"What-if" Wildfire scenario

Wildfire directly influences vegetation dynamics, but also has influences on soil properties such as hydrophobicity, infiltration, and runoff. A literature search for how wildfire is modeled, as well as a search for information on wildfires in the region of the study area indicated that infiltration and ET are greatly influenced by fire severity and by fire temperature (Krammes and DeBano 1965, Scott and Van Wyk 1990, Neary et al. 2003, Beyers et al. 2005, Rau et al. 2005). Literature suggests that decreases in soil infiltration can result in higher runoff depending on the soil type, severity of fire, and the amount of surface area that was burned (Krammes and DeBano 1965).

Wildfire data were obtained from the California Fire Resources Assessment Program online database for Mono County California, where the upper West Walker River basin is located. A Geographic Information System (GIS) was used to identify wildfires within the watershed boundary using a watershed boundary shapefile obtained from Scotty Strachan at the University of Nevada, Reno.

Wildfire data consisted of the date when fire occurred (fire season), and the location of fire within the watershed. Additional data including burn area and duration of fire were accessed using GIS, however these data were inconsistent and were not used for wildfire analysis on streamflow. Because the model is applied to the entire watershed equally, the exact location of the fire was not used in analysis of wildfire effect on streamflow, and fire was assumed to apply to the entire watershed.

Average parameter values from all 500 Monte Carlo simulations from the best model were used for this scenario. Once fire seasons had been determined, the model was

adjusted to reflect estimates of increased runoff. Runoff was adjusted to be between 12% and 32% higher, as suggested by literature (Osborn et al. 1964, Krammes and DeBano 1965), and was represented for this model by increasing parameter *a* by 0.12. This parameter was applied to the dry season when fire occurred as well as the wet season immediately following the fire.

In addition to affecting runoff, fire affects ET in two ways. First, evaporation typically increases after a fire because shading from plant canopy is reduced, resulting in higher surface temperatures. This reduces water availability for infiltration. Secondly, removing vegetation in a watershed severely reduces transpiration. Reduction in transpiration rates can, in some cases, be directly proportional to the fraction of vegetation lost due to wildfire (Wohlegemuth et al. 2006). Unless the fire severity is minimal, the decrease in transpiration will be greater than the increase in evaporation, resulting in lower overall ET after a wildfire event. Thus, to simulate wildfire effects on ET, ET estimates were decreased by 20% across the entire watershed by reducing parameter *b* in the model by 0.2. Similar to the parameter *a* adjustment, the reduced parameter *b* was applied only to the dry season when wildfire occurred and wet season immediately following. Once parameters were adjusted for wildfire based on documented occurrences generated using GIS, overall r^2, RMSE and %bias were calculated to evaluate effects of wildfire on estimating streamflows. In addition, these parameters were calculated between the original model and the revised wildfire model to see how sensitive the model was to these changes.

CHAPTER 3: RESULTS & DISCUSSION

Model error and uncertainty

Many factors contribute to sources of error in water balance model predictions, including the number of model parameters, model equations, model structure and error associated with input data, or any measurements and estimations (Atkinson et al. 2002, Farmer et al. 2003, Butts et al. 2004, Oudin et al. 2006). The very nature of modeling can often over-simplify model parameters, introducing error into the model, and causing it to fail to reproduce complex and interdependent hydrologic processes (Atkinson et al. 2002, Farmer et al. 2003, Butts et al. 2004, Oudin et al. 2006). For example, in this modeling project the assumption that model parameters are constant over time and space is a simplification that introduces error (Atkinson et al. 2002, Wagener et al. 2003).

Difficulty extrapolating precipitation measurements across an entire watershed can lead to an over- or under-prediction of runoff in models as well. However, use of extrapolated values for precipitation from PRISM (Daly et al. 1994) resulted in streamflow representation that reflected observed streamflow fairly well in the upper West Walker River basin (Saito et al. 2008), and can be very useful when instrumental precipitation or air temperature data are not available or representative of the basin. There is also the assumption that any instrumental records available and used for reconstructions are representative of historic climate data throughout the reconstruction period (Saito et al. 2008, Sheppard 2010).

Another problem when comparing between simulated streamflow and observed

streamflow for calibration of the model is that a good fit of the simulated to observed data can be made with unrealistic parameter values (Boyle et al. 2000). These errors can occur when measures such as RMSE or r^2 are used to evaluate model performance without the use of other performance metrics. For example, use of r^2 is a common statistic for comparing simulated streamflow to observed streamflow, but it is a measurement of representing trends and not necessarily how well modeled the magnitude of results compare to the magnitude of observed flow measurements (Wagener et al. 2003). Thus, the use of multiple objective statistical functions is recommended to increase the ability to evaluate model performance. For example, the use of annual, seasonal, or monthly streamflow bias calculations can be used in conjunction with RMSE and r^2 calculations (Boyle et al. 2000, Wagener et al. 2003) as was done in this study.

Model performance

For Model A, the best performing model and temperature scheme was Model A_{ave} using average seasonal temperature, with the worst performing being Model A_{min} (Table 3). Model A_{ave} had the highest seasonal r^2 for both seasons, the best wet season RMSE, the lowest overall %bias, the lowest overall average RMSE. Model B_{max} using maximum seasonal temperatures performed the best for Model B according to statistical measures. Model B_{ave} performed the worst, with the highest RMSE and lowest r^2. Model B_{max} had the lowest dry season RMSE and dry season %bias at 9.57 cm and -1.28%, respectively.

According to dry season %biases all models were better at estimating streamflow in the dry season than in the wet (Table 3). The Model that best simulated dry season

streamflow was Model B_{max}. This model under-predicted streamflow by 1.28%. Overall, the model that had the lowest overall %bias for all seasons was Model A_{ave}, over-predicting streamflow between WY 1940 and WY 2006 by 0.66%.

Over-estimation of streamflow during the wet season for most of the models could have been a result of inappropriate seasonal temperature representation, as seen with Model A_{max} and Model B_{max} over-predicting seasonal streamflow by more than 26.00%. These models used maximum seasonal temperatures, and not only did the temperature influence precipitation, with all precipitation being rain, resulting in a lack of snowmelt, but both Model A_{max} and Model B_{max} did not produce runoff (a = 0.00) for any simulations. The lack of snow precipitation is unrealistic, since snow is the primary source of water contributing to dry season streamflow in this region of the U.S. (Stewart et al. 2004, Maurer 2007, Maurer et al. 2007, Day 2009, Hidalgo et al. 2009, Clow 2010).

Averaged seasonal temperatures resulted in an average runoff fraction (a) ranging from 0.00 for Model A_{max} and Model B_{max} to 0.64 for Model A_{ave}, whereas minimum seasonal temperatures resulted in average runoff fractions of 0.19 for Model B_{min} and 0.47 for Model A_{min} (Figure 7). As mentioned previously, the 500 simulations using the Monte Carlo-styled approach indicated that parameter estimates for Model A_{max} and Model B_{max} were unrealistic, so no further discussion of the parameters is made for those models. The ranges simulated for all other models' parameter a were lower than the 0.74 found in Saito et al. (2008). A possible explanation for the reduced a values in Model A and Model B compared to Saito et al. (2008) could be the incorporation of a snow component, which directly influences the form of precipitation available for contribution

to runoff. Snow precipitation would not be available for runoff until temperature increased enough to allow melt to occur. Ponce and Shetty's (1995) analysis of water balances in different regions of the world indicates runoff coefficients are typically lower than the *a* values found in this study for regions with annual precipitation of less than 100 mm/year. The low *a* values estimated in this study indicate that much more of the seasonal precipitation is treated as infiltration, meaning more water is available for ET, infiltration, GW flow, and baseflow. However, Ponce and Shetty's (1995) model was annual and did not account for snow. The water balances were also done on a spatial scale much larger than the upper West Walker River Basin. The low *a* value seen in Solander et al. (2010) can possibly be accounted for by the fact that dry season was not modeled and streamflow diversions were present upstream.

For parameter *b*, Saito et al. (2008) reported a value of 0.38, with Solander reporting 0.70 with the addition of a snowmelt component. In this study, *b* average values ranged from 0.02 to 0.29 for Model A, and were estimated at between 0.01 and 0.02 for all temperatures for Model B (see Figure 7). Thus, average *b* values for this study resulted in a lower proportion of the infiltrated water treated as ET as compared to the previous studies. Although the parameter was lower, the amount of ET may have been similar. ET estimates from the models were compared to the California Irrigation Management Information System (Jones 1999) for Zone 11, Central Sierra Nevada. Seasonal comparisons of ET for Model A and Model B to CIMIS (Jones 1999) seasonal ET references indicate that even the highest seasonal ET estimates of 18.73 cm during the wet season of WY 1982 for Model A_{min}, was just over half of CIMIS estimates for wet

season ET (36.22 cm/season). The other models estimated a maximum ET of less than 3 cm/season. ET values ranged from 0.08-21.43 cm/year in Saito et al. (2008) and 5.58-31.40 cm for the months October-May in Solander et al. (2010). Shevenell (1996) estimates ET for the dry season at 125.86 cm and for the wet season at 16.13 cm for Region 2, where the upper West Walker River basin is located. Thus simulated wet season ET is similar for Model A_{min}, but extremely low for the other models. In addition, dry season ET estimates were consistently lower than wet season estimates through every model. Shevenell (1996) estimates that ET for Region 2 (Topaz Lake, NV) greater than 2000 m elevation for February through November would approach zero where temperatures are below 0.00 ^{o}C or there is the presence of snow. Since the entire upper West Walker River basin is above 2000 m elevation (lowest elevation: 2031 m) and often has snow present after February, lower ET estimates predicted by the model could therefore be much lower than the 125.86 cm estimated by Shevenell (1996).

Average "best" estimates for parameter *c* ranged between 0.22 (Model A_{ave}) to 0.77 (Model A_{max}). These were significantly higher than both Saito et al. (2008), 0.0, and Solander et al. (2010), also 0.0. Due to parameters *a* and *b* having lower estimates in both Model A and Model B, we might expect to see higher values for *c*, as well as *d*, since precipitation was not contributing very much to runoff or ET. However, smaller fractions can represent higher volumes. Average values for parameter *d* ranged from 0.13 (Model B_{ave}) to 0.74 (Model A_{ave}). Parameter *d* increased from 0.39 in Saito et al. (2008) to 0.57 in Solander et al. (2010) with both values falling within the ranges generated with Model A and Model B (see Figure 7).

Initial groundwater storage (GS_i) estimates in the model decreased from approximately 127 cm in Saito et al. (2008) to between 10.62 cm and 42.64 cm for Models A and B using all temperatures. Initially, no boundary conditions were set for GS_i other than that it had to be greater than 0.0 cm. After unrealistic GS_i values were estimated, an upper bound of 100 cm was set to prevent spikes in streamflow seen during the first season simulations in Model B.

Parameter *m*, representing the maximum melt rate (%), had an average value over 500 simulations in Model B_{max} of 0.57, or 57%, similar to the value suggested for use by McCabe and Markstrom (2007) of 0.5 (Figure 8). Parameter *m* was higher for Model B_{ave} and Model B_{min}, averaging 0.62 (62%) and 0.85 (85%) over 500 simulations, respectively. Comparison between parameters influencing snow precipitation and melt could not be made with the Saito et al. (2008) model due to that model not incorporating a snow component. The method for determining snow and melt in Solander et al. (2010) used a temperature-index approach, making direct comparison with that model inappropriate as well. Solander et al. (2010) also did not model the dry season due to the fact that streamflow is diverted from the system to be utilized for irrigation, altering natural flow used for calibration during that season.

Estimates for Model B_{ave} indicated that parameters *a* and *c* were not very robust, ranging across the spectrum of boundary conditions (see Table 3 and Figure 7). This is also seen in *b*, *c*, and *d* in Model A_{min}, and to a lesser extent for parameters *a*, *c*, and *d* in Model B_{min}, and parameters *b*, *c* and *d* in Model A_{ave}. Parameter *b* represented the ET coefficient in this model, and was very close to zero across all models except Model A_{min},

where parameter *b* was 0.29. The most robust parameter estimate was seen for Model A_{ave}, where parameter *a* was consistently between 0.56 and 0.66, with an average value of 0.64 ± 0.02 over 500 model simulations. A runoff factor of 0.64 would be more consistent with soil conditions described earlier for this basin. Snow component parameters (*e*, *f*, *s*, *w* and *m*) were not very robust, though average estimates over the 500 simulations were considered reasonable (Figure 8 and 9).

Figure 7. Results of parameter estimation process for Model A and Model B using all temperature schemes for parameters *a*, *b*, *c*, and *d*.

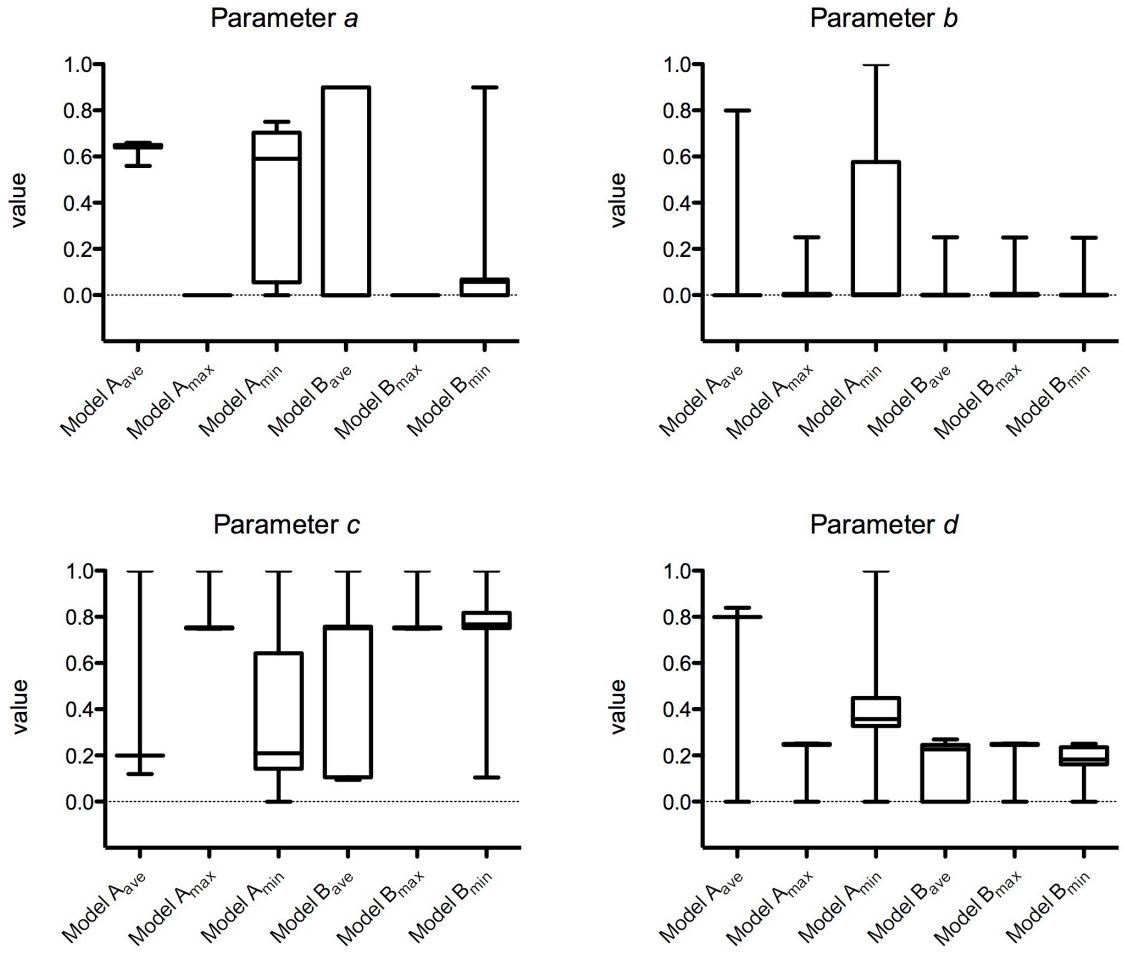

Table 3. Results of Monte Carlo simulations using PRISM data for input. Values shown are average ± one standard deviation, with ranges of values over the 500 simulations in parentheses. "*n*" = number of seasons modeled; "Std" is the standard deviation.

Model A_{ave}	
Parameter (units)	500 Simulation results
n	134
a	0.64 ± 0.02 (0.56-0.66)
b	0.05 ± 0.14 (0.00-0.80)
c	0.22 ± 0.09 (0.12-1.00)
d	0.74 ± 0.16 (0.00-0.84)
s (°C)	3.25 ± 0.89 (0.47-3.89)
w (°C)	0.57 ± 0.37 (0.19-3.69)
GSi (cm)	12.73 ± 16.54 (0.00-97.07)
r^2	0.90 ± 0.02 (0.82-0.90)
RMSE (cm)	7.50 ± 0.74 (7.27-10.04)
Overall %Bias	0.66 ± 1.53 (-3.63-5.79)
Wet r^2	0.28 ± 0.06 (0.06-0.31)
Wet RMSE (cm)	3.74 ± 1.17 (3.33-7.71)
Wet %Bias	-0.95 ± 4.20 (-9.66-13.41)
Dry r^2	0.78 ± 0.04 (0.64-0.80)
Dry RMSE (cm)	9.90 ± 0.60 (9.71-12.04)
Dry %Bias	2.28 ± 1.20 (-1.93-2.72)
Ave Q_{sim} (cm)	26.36 ± 0.12 (25.93-26.43)
Std Q_{sim} (cm)	21.70 ± 0.17 (21.11-21.96)
Ave Q_{obs} (cm)	25.90
Std Q_{obs} (cm)	23.51

Model B_{ave}	
Parameter (units)	500 Simulation results
n	134
a	0.40 ± 0.45 (0.00-0.90)
b	0.01 ± 0.04 (0.00-0.25)
c	0.49 ± 0.33 (0.09-1.00)
d	0.13 ± 0.12 (0.00-0.27)
e (°C)	1.98 ± 1.06 (0.20-3.89)
f (°C)	1.44 ± 0.93 (0.00-3.69)
m (MeltMax)	0.62 ± 0.43 (0.13-1.00)
GSi (cm)	42.64 ± 39.93 (0.00-100.00)
r^2	0.70 ± 0.21 (0.06-0.90)
RMSE (cm)	15.52 ± 8.12 (8.07-26.33)
Overall %Bias	5.25 ± 24.53 (-23.81-29.59)
Wet r^2	0.11 ± 0.08 (0.01-0.32)
Wet RMSE (cm)	5.42 ± 1.23 (3.81-11.92)
Wet %Bias	40.41 ± 17.25 (18.05-64.97)
Dry r^2	0.49 ± 0.30 (0.14-0.78)
Dry RMSE (cm)	20.77 ± 12.32 (9.40-35.27)
Dry %Bias	-29.92 ± 31.92 (-67.68- -1.20)
Ave Q_{sim} (cm)	20.70 ± 7.72 (11.83-27.68)
Std Q_{sim} (cm)	13.31 ± 7.37 (4.75-19.94)
Ave Q_{obs} (cm)	25.90
Std Q_{obs} (cm)	23.51

Model A_{max}	
Parameter (units)	500 Simulation results
n	134
a	0.00 ± 0.00 (0.00-0.00)
b	0.02 ± 0.06 (0.00-0.25)
c	0.77 ± 0.06 (0.75-1.00)
d	0.23 ± 0.06 (0.00-0.25)
s (°C)	1.63 ± 0.79 (0.20-2.69)
w (°C)	0.60 ± 0.65 (0.00-2.39)
GSi (cm)	10.62 ± 5.94 (0.00-30.16)
r^2	0.90 ± 0.00 (0.89-0.90)
RMSE (cm)	8.14 ± 0.02 (8.12-8.25)
Overall %Bias	26.92 ± 0.42 (26.08-28.54)
Wet r^2	0.04 ± 0.00 (0.03-0.05)
Wet RMSE (cm)	6.39 ± 0.06 (6.35-6.65)
Wet %Bias	55.16 ± 0.90 (53.44-58.63)
Dry r^2	0.77 ± 0.00 (0.77-0.78)
Dry RMSE (cm)	9.57 ± 0.00 (9.56-9.59)
Dry %Bias	-1.31 ± 0.06 (-1.55- -1.15)
Ave Q_{sim} (cm)	27.62 ± 0.02 (27.54-27.69)
Std Q_{sim} (cm)	19.83 ± 0.04 (19.68-19.91)
Ave Q_{obs} (cm)	25.90
Std Q_{obs} (cm)	23.51

Model B_{max}	
Parameter (units)	500 Simulation results
n	134
a	0.00 ± 0.00 (0.00-0.00)
b	0.02 ± 0.05 (0.00-0.25)
c	0.76 ± 0.05 (0.75-1.00)
d	0.24 ± 0.05 (0.00-0.25)
e (°C)	1.68 ± 0.91 (0.20-3.77)
f (°C)	0.76 ± 0.81 (0.00-3.57)
m (MeltMax)	0.57 ± 0.38 (0.00-1.00)
GSi (cm)	11.28 ± 6.12 (0.00-33.73)
r^2	0.89 ± 0.00 (0.89-0.90)
RMSE (cm)	8.14 ± 0.03 (8.08-8.28)
Overall %Bias	26.96 ± 0.41 (26.10-28.37)
Wet r^2	0.04 ± 0.00 (0.03-0.04)
Wet RMSE (cm)	6.40 ± 0.06 (6.36-6.77)
Wet %Bias	55.20 ± 0.88 (53.44-58.30)
Dry r^2	0.77 ± 0.00 (0.77-0.78)
Dry RMSE (cm)	9.57 ± 0.02 (9.46-9.66)
Dry %Bias	-1.28 ± 0.06 (-1.57- -1.08)
Ave Q_{sim} (cm)	27.62 ± 0.02 (27.53-27.72)
Std Q_{sim} (cm)	19.83 ± 0.04 (19.70-19.92)
Ave Q_{obs} (cm)	25.90
Std Q_{obs} (cm)	23.51

Model A_{min}	
Parameter (units)	500 Simulation results
n	134
a	0.47 ± 0.28 (0.00-0.75)
b	0.29 ± 0.37 (0.00-1.00)
c	0.32 ± 0.25 (0.00-1.00)
d	0.40 ± 0.21 (0.00-1.00)
s (°C)	2.07 ± 1.54 (0.35-3.89)
w (°C)	1.27 ± 1.03 (0.15-3.69)
GSi (cm)	39.33 ± 29.52 (0.12-99.95)
r^2	0.71 ± 0.17 (0.46-0.90)
RMSE (cm)	12.30 ± 3.56 (8.14-17.47)
Overall %Bias	10.58 ± 10.90 (-0.35-42.56)
Wet r^2	0.03 ± 0.01 (0.00-0.04)
Wet RMSE (cm)	7.13 ± 1.93 (5.40-14.20)
Wet %Bias	26.79 ± 22.66 (1.01-102.80)
Dry r^2	0.45 ± 0.30 (0.00-0.78)
Dry RMSE (cm)	15.54 ± 5.62 (9.46-24.01)
Dry %Bias	-5.63 ± 5.04 (-18.00- -0.73)
Ave Q_{sim} (cm)	25.66 ± 1.17 (23.98-27.65)
Std Q_{sim} (cm)	19.93 ± 1.24 (16.62-24.45)
Ave Q_{obs} (cm)	25.90
Std Q_{obs} (cm)	23.51

Model B_{min}	
Parameter (units)	500 Simulation results
n	134
a	0.19 ± 0.33 (0.00-0.90)
b	0.01 ± 0.03 (0.00-0.25)
c	0.68 ± 0.26 (0.10-1.00)
d	0.16 ± 0.09 (0.00-0.25)
e (°C)	2.66 ± 1.66 (0.20-3.89)
f (°C)	1.09 ± 0.97 (0.00-3.69)
m (MeltMax)	0.85 ± 0.33 (0.14-1.00)
GSi (cm)	24.93 ± 33.78 (0.00-100.00)
r^2	0.80 ± 0.21 (0.16-0.91)
RMSE (cm)	10.71 ± 6.72 (7.21-25.63)
Overall %Bias	4.28 ± 14.22 (-20.30-27.67)
Wet r^2	0.12 ± 0.07 (0.00-0.32)
Wet RMSE (cm)	4.89 ± 1.06 (3.88-8.36)
Wet %Bias	20.20 ± 19.00 (1.16-57.92)
Dry r^2	0.66 ± 0.26 (0.09-0.78)
Dry RMSE (cm)	14.05 ± 9.87 (9.43-35.87)
Dry %Bias	-11.65 ± 25.86 (1.22- -68.75)
Ave Q_{sim} (cm)	24.04 ± 5.65 (11.75-27.66)
Std Q_{sim} (cm)	18.42 ± 6.70 (4.76-21.99)
Ave Q_{obs} (cm)	25.90
Std Q_{obs} (cm)	23.51

Figure 8. Results of parameter estimation process for Model B using all temperature schemes for parameters *e*, *f* and *m*.

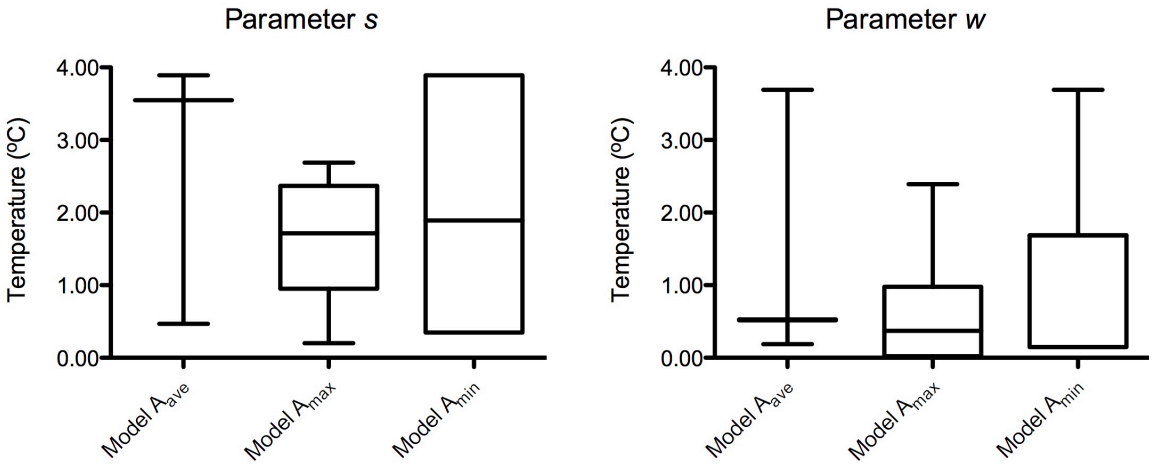

Figure 9. Results of parameter estimation process for Model A using all temperature schemes for parameters *s* and *w*.

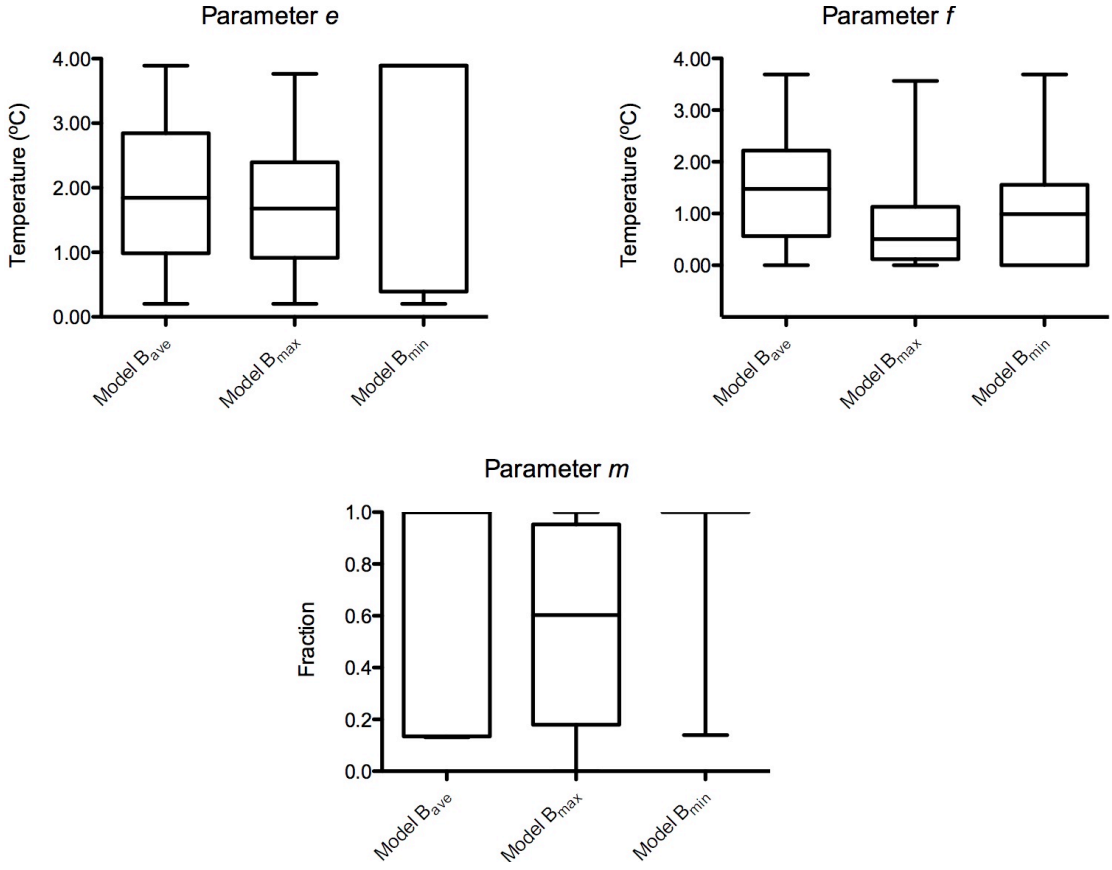

Once the Monte Carlo simulations were completed, averages of the 500 simulations were calculated for each parameter value for each model. The averaged parameter values were then put into each corresponding model and simulated streamflow was plotted against observed streamflow for the period between WY 1940-2006 and resulting statistics were calculated (Table 4). Initial parameter values randomly generated during the Monte Carlo simulations were also investigated to determine the influences of individual parameters on each performance metric (Appendix, Figures 18-29).

Table 4. Summary of model results using parameter values averaged over 500 Monte Carlo simulations for Models A and B with all temperature schemes. Values in bold represent the best outcome of the metric over all models.

	r^2	RMSE (cm)	overall bias (%)	est ave (cm)	std dev (cm)	Wet r^2	Wet RMSE (cm)	wet bias (%)	Dry r^2	Dry RMSE (cm)	dry bias (%)
Observed Q				25.90	23.51						
Model A_{ave}	**0.90**	**7.29**	**0.90**	**26.43**	21.66	0.28	**3.40**	**-0.73**	**0.80**	9.73	2.52
Model A_{max}	**0.90**	8.13	27.48	27.75	19.92	0.04	6.41	55.80	0.77	**9.55**	**-0.84**
Model A_{min}	0.01	27.65	109.12	23.56	12.33	0.02	22.93	275.11	0.08	31.68	-56.86
Model B_{ave}	0.00	24.05	90.97	22.36	5.76	**0.35**	17.80	236.31	0.69	28.98	-54.37
Model B_{max}	**0.90**	8.13	27.37	27.71	19.89	0.04	6.40	55.68	0.77	9.56	-0.95
Model B_{min}	0.78	15.53	50.88	23.36	10.03	0.26	10.85	135.16	0.78	19.09	-33.40

The plot for Model A_{ave} shows a very good fit (Figure 10), with an r^2 of 0.90, RMSE of 7.29 cm, and wet season and dry season %bias of -0.73 and 2.52, respectively. This model had the lowest overall %bias, representing streamflow very well. Using averaged parameter values for Model A_{max} indicated that the averaged parameter values for this model did a good job representing streamflow trends (Figure 11), and this model had a

high r^2 (0.90), and low RMSE (8.13 cm). However, Model A_{max} using averaged parameter values over-predicted streamflow by 27.48% over the period beginning in WY 1940 and ending in WY 2006.

Figure 10. Model A_{ave}, the simple water balance model with WASMOD snow calculations incorporating average seasonal temperatures.

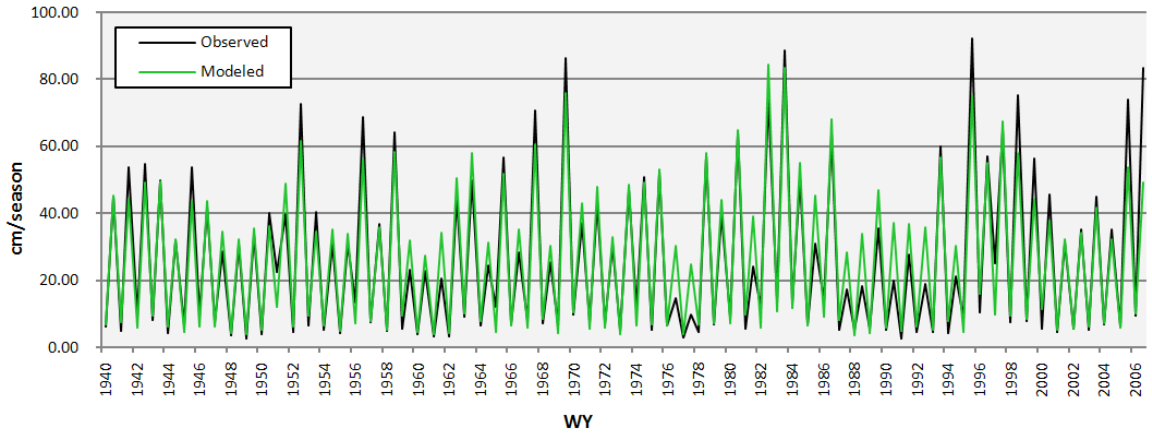

Figure 11. Model A_{max}, the simple water balance model with WASMOD snow calculations incorporating maximum seasonal temperatures.

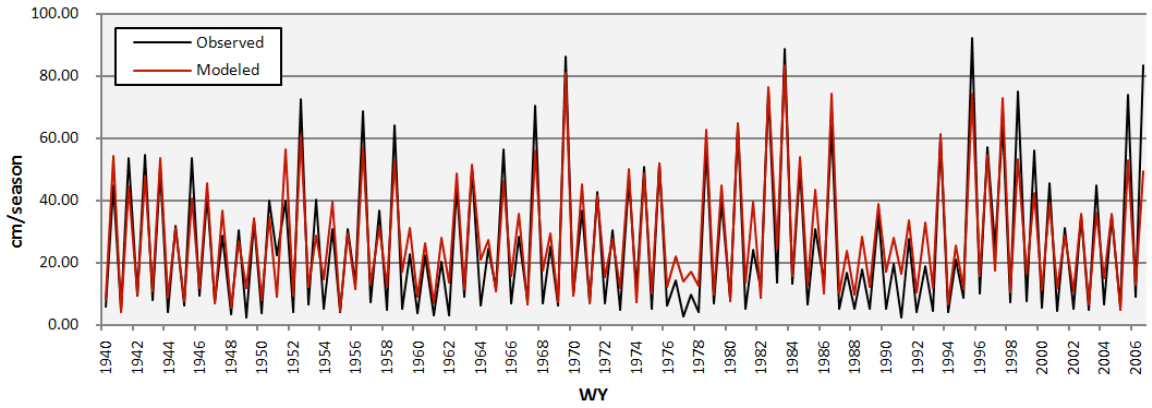

The plot for Model A_{min} shows a poor fit (Figure 12), with an r^2 of 0.01, RMSE of 27.65 cm, and the overall %bias is much higher, at 109.12%, an indication of over-prediction for simulated streamflow. This model had the highest overall %bias when averaged parameter values were used, represented streamflow very poorly, and does not represent the physical processes influencing streamflow well.

Figure 12. Model A_{min}, the simple water balance model with WASMOD snow calculations incorporating minimum seasonal temperatures.

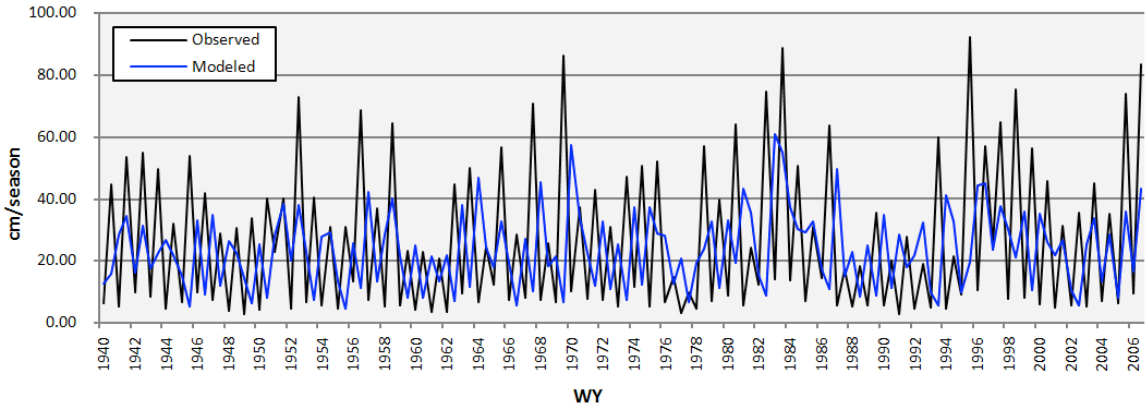

The plot for Model B_{ave} with averaged parameter values shows a poor fit (Figure 13), with an r^2 of 0.00, RMSE of 24.05 cm. This model had the second highest overall %bias and the second highest seasonal %bias values for both wet and dry seasons, representing streamflow very poorly. Thus, the averaged parameter values for this model did not do a good job representing appropriate observed streamflows.

Figure 13. Model $B_{ave,}$ the simple water balance model with Thornthwaite snow calculations incorporating average seasonal temperatures.

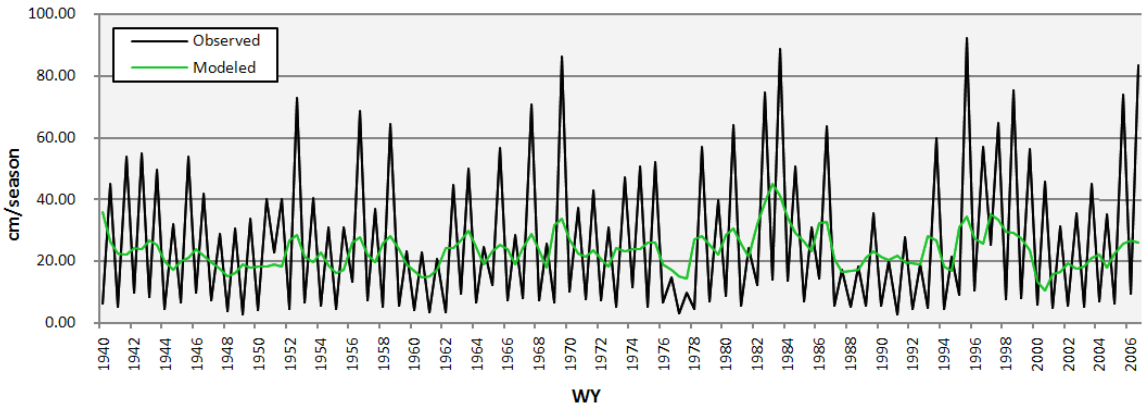

Using averaged parameter values for Model B_{max} indicated that the averaged parameter values for this model did a good job representing streamflow trends (Figure 14), and this model had a high r^2, and low RMSE. However, Model B_{max}, like Model A_{max}, using averaged parameter values over-predicted streamflow, in this case by 27.37% over the period beginning in WY 1940 and ending in WY 2006. Results between Model A_{max} and Model B_{max} were very similar.

Figure 14. Model B_{max}, the simple water balance model with Thornthwaite snow calculations incorporating maximum seasonal temperatures.

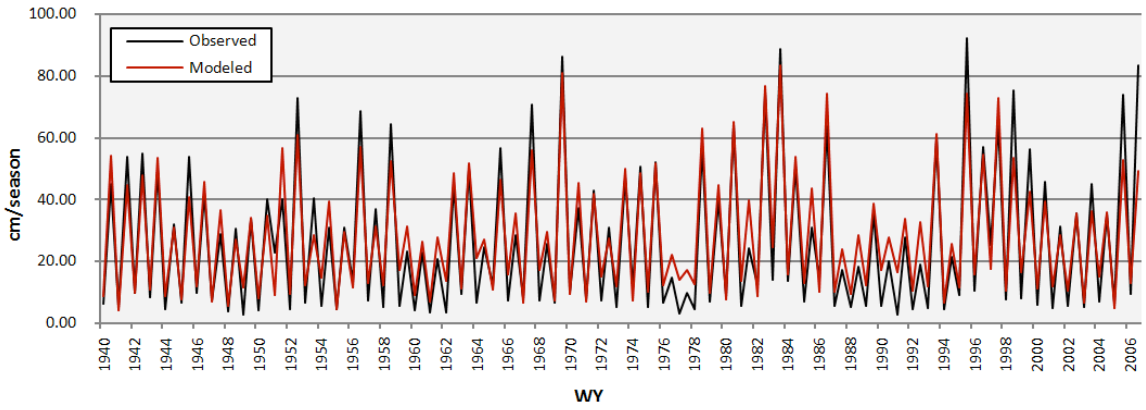

Using averaged parameter values for Model B_{min} resulted in a poor representation of observed streamflows (Figure 15), or representing appropriate ranges for estimated parameters.

Figure 15. Model B_{min}, the simple water balance model with Thornthwaite snow calculations incorporating minimum seasonal temperatures.

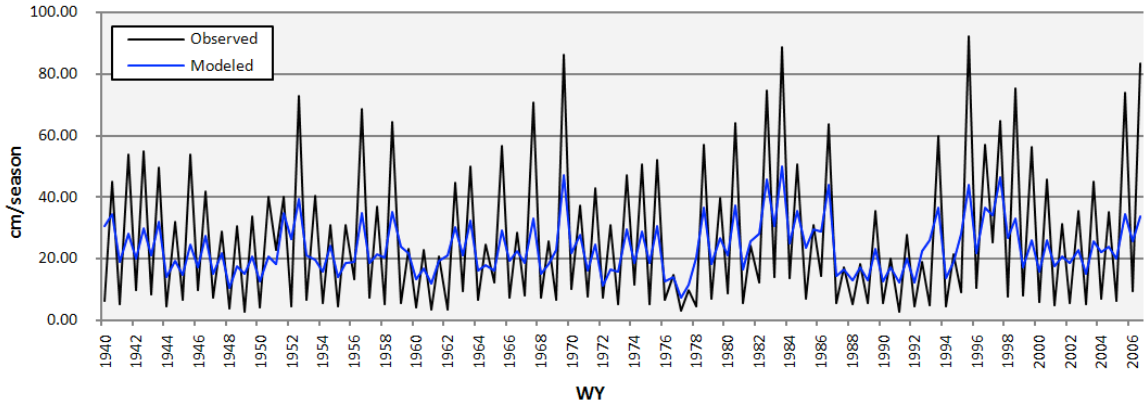

The r^2 from simulated streamflow for all models except Model A_{min}, Model B_{ave}, and Model B_{min} were slightly better than in Saito et al. (2008) ($r^2 = 0.87$) and Solander et al. (2010) ($r^2 = 0.81$) . One possible explanation for lower r^2 for Model A_{min}, Model B_{ave}, and Model B_{min}, is that in all of these models wet season streamflow was not represented well. r^2 values were very low during wet season, at 0.02, 0.35, and 0.26, respectively. Since precipitation primarily falls during the wet season in this region, one would expect to see that precipitation stored as snowpack, but instead we see greater snowmelt, resulting in a higher simulation of streamflow. Model A_{ave} had a high r^2 value, but also represented snow precipitation, snowmelt, and runoff, resulting in a very good simulation of streamflow for both seasons as compared to observed streamflow.

Assessment of best model for use with proxy data

Once Monte Carlo simulations for Model A and Model B with all temperatures were completed, all models were compared to determine best model performance (see Table 4). Model A_{ave} was chosen as the most appropriate model to use with proxy data based on lowest RMSE, highest r^2, and lowest overall %bias. Importantly, Model A has 1 fewer parameter than Model B, and is considered to be the more parsimonious model, accounting for the same physical processes with greater simplicity, while also performing the best when using only air temperature and precipitation data as input. Thus, Model A_{ave} was chosen as the most appropriate model to use with proxy tree-ring air temperature and precipitation data and was also used for simulating wildfire in the upper West Walker River.

"What-if" wildfire scenario

GIS analysis for the upper West Walker River basin indicated 14 wildfires occurred during the period between WY 1940 and 2006 with no fires recorded prior to 1961 in this basin (Figure 16). All wildfires occurred during the dry season. Seven fires occurred during the dry season of 1991 at various locations in the watershed.

Figure 16. Wildfires in the upper West Walker River basin between WY 1940 and 2006.

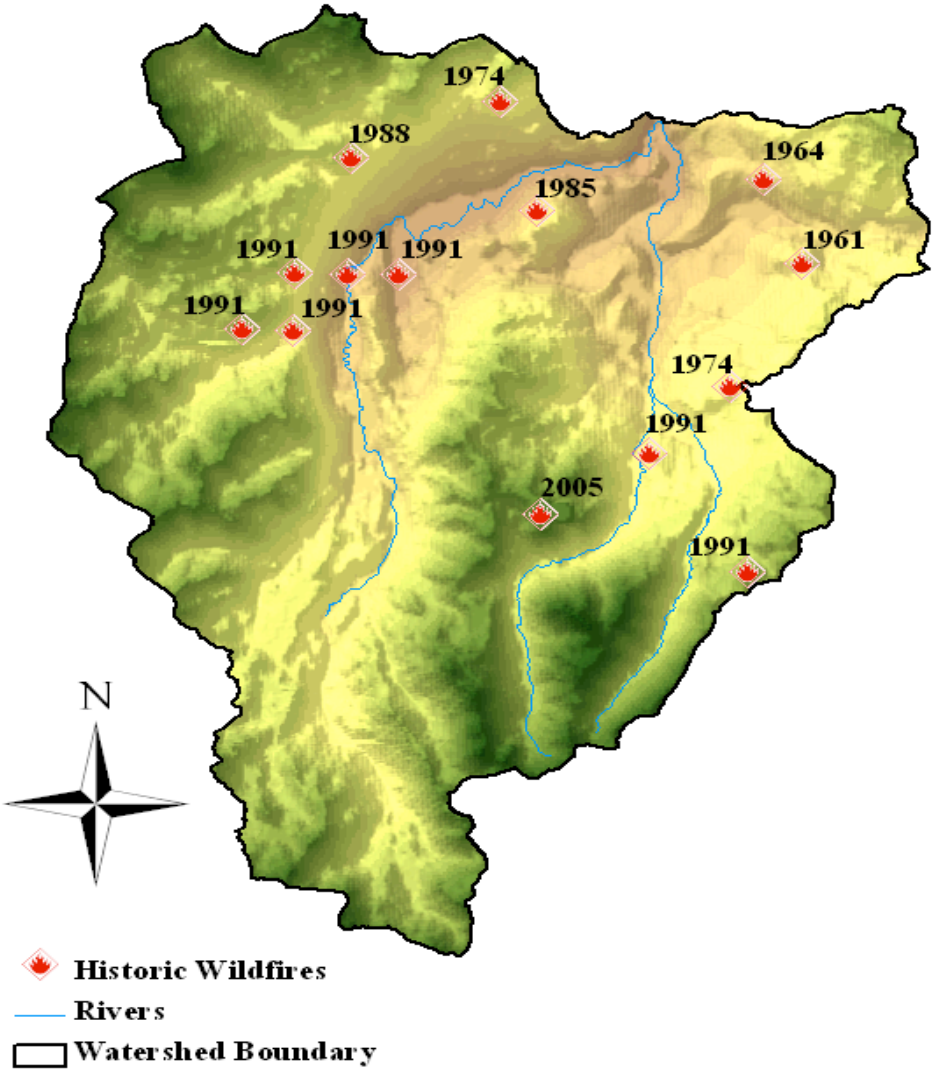

Results from the wildfire scenario were compared to observed streamflow during recorded fire seasons, as well as to Model A_{max} simulated streamflow during recorded fire seasons (Table 5). Comparison was also made over the entire period of record between WY 1940 and 2006. When parameters reflecting wildfires were used in Model A_{ave} between WY 1940 and WY 2006, an overall r^2 of 0.85, was obtained, which was lower than Model A_{ave} without the wildfire parameter adjustments (Figure 17).

Figure 17. Simulated streamflow incorporating wildfire effects compared to observed streamflow for the period between 1960 and 2006. Arrows indicate seasons when wildfire occurred. No wildfire was recorded in this basin prior to 1961.

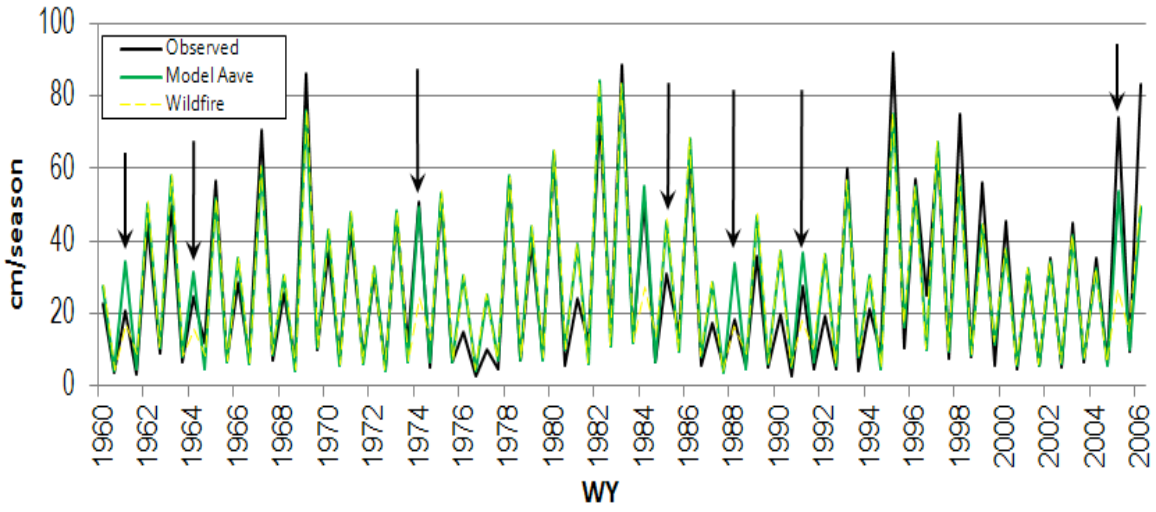

The RMSE was 9.02 cm, slightly higher than Model A_{ave}. The overall %bias was 1.57%, which was worse than Model A_{ave} without wildfire parameter changes, but still a very good simulation of streamflow (Table 5).

Table 5. Statistical measures for wildfire simulation compared to Model A_{ave} results.

Model	r^2	RMSE (cm)	Overall %Bias	Ave Q_{sim} (cm)	Std Q_{sim} (cm)
Model A_{ave}	0.90	7.50	0.66	26.36	21.70
Wildfire	0.85	9.02	1.57	25.39	20.97

Overall, incorporating wildfire parameter adjustments resulted in greater overall %bias, a lower r^2, and slightly higher RMSE. Average streamflow for the wildfire simulation worsened slightly compared to observed streamflow for the modeling period, from 26.36 cm for Model A_{ave} to 25.39 cm for the wildfire simulation, as compared to the observed average of 25.90 cm.

Comparisons of the averages from wildfire seasons relative to the observed streamflow and Model A_{ave} indicate not only that the wildfire seasons generally had lower streamflow, but that the wet season immediately following wildfire generally had higher streamflow than Model A_{ave} simulated streamflow (Table 6). Wildfire simulated streamflow was less than observed in all dry seasons when wildfire occurred, and greater than observed streamflow during the wet season following a fire episode. This can be seen when streamflow is plotted for observed, Model A_{ave}, and wildfire seasons (see Figure 14). The model appears to be overestimating streamflow for the subsequent wet season.

Table 6. Observed, Model A_{ave} simulated, and Wildfire simulated streamflow (cm/season) for the dry season when wildfire occurred and wet season immediately following.

Year	Season	Observed	Model A_{ave}	Wildfire
1961	Dry	20.37	34.33	16.82
1962	Wet	3.22	4.60	8.37
1964	Dry	56.45	31.51	25.43
1965	Wet	7.12	4.78	11.98
1974	Dry	50.66	49.15	24.08
1975	Wet	5.18	6.94	12.16
1984	Dry	50.56	55.03	27.10
1985	Wet	6.64	6.86	13.13
1988	Dry	18.06	34.04	16.65
1989	Wet	5.45	4.52	8.29
1991	Dry	27.59	36.90	18.08
1992	Wet	4.41	6.57	9.78
2005	Dry	73.87	75.12	26.38
2006	Wet	9.32	16.48	14.61

Had Model A_{ave} been consistently under-predicting streamflow, an adjustment of parameters to reflect wildfire may have produced better estimates of streamflow.

However, this was not the case, so incorporation of wildfire moved estimates slightly further away from observed streamflow, which may have been a result of Model A_{ave} having already taken into account wildfire during the parameter estimation process. In addition, wildfire may have been over-estimated because wildfire was assumed to influence the entire watershed for this study.

A disadvantage of modeling wildfire in this basin was that the wildfire data acquired for the upper West Walker River basin were missing burn area for almost all fires historically recorded. In addition, a spatial component was not available in this modeling approach to account for the size of wildfires even if data were available. For this modeling scenario only ET and runoff parameters were adjusted to reflect effects due to wildfire. However, wildfire can also alter snowmelt and snow accumulation patterns, which were not accounted for through this modeling approach. These wildfire influences are similar to increased air temperature effects on snowmelt and accumulation patterns. Accumulation of snow tends to be higher in areas burned by wildfire, and timing and amount of snowmelt can be greatly influenced by lack of vegetation. Reduction in vegetation canopy cover exposes snow to greater solar radiation, resulting in both earlier and faster snowmelt during a season (Wohlegemuth et al. 2006). To better understand how wildfire influences streamflow another parameter could have been introduced to address snow melt, or the temperature threshold parameter accounting for melt (w) could have been adjusted to reflect changes in vegetation that influence solar radiation influences on snowpack. This might be in the form of lowering the threshold to a level that would generate greater snowmelt availability in the simulations.

CHAPTER 4: CONCLUSIONS

Overall, the simple water balance modeling approach with a seasonal snow component was very successful. The simplicity of the WASMOD snow component allowed only air temperature and precipitation to be used as input data, thus making it suitable for use with proxy tree-ring data. The model also performed very well with only those two input data, suggesting the appropriateness for use when little data are available.

The lack of water diversions from the watershed in this basin removed the complications seen in Solander et al. (2010), and contributed to the model's success by allowing the ability to model each season by comparing to natural flow. The inclusion of a snow component also improved streamflow simulation over the Saito et al. (2008) model, which did not take into account snow or snowmelt, and operated annually rather than seasonally. Furthermore, the results of this study should be considered a beneficial tool for reconstructing past streamflow.

Developing proxy tree-ring data for air-temperature and precipitation for future use with this model is one of the main areas of future work needed to complete this project. Proxy tree-ring data have the potential to extend the period of record back many centuries, and when used as model input, can greatly improve understanding of past streamflow in this basin. Additional work is also required to relate tree-ring data with seasonal temperatures for use in modeling snow precipitation and melt.

It would also be beneficial to test this model in similar watersheds to determine how well the model can reproduce long-term hydrologic fluctuations elsewhere, and to

evaluate the model's ability to be generalizable. Preferably, the model would be successful when applied to other basins that have long measured streamflow records and more basin-specific physical measurements of hydrologic variables, in order to provide better parameter estimates for this model.

Model A_{ave} was ultimately deemed the best model for use with proxy tree-ring data. The similarities between Model A and Model B indicate that several models simulated streamflow well with different seasonal air temperature inputs, however, the lack of snow precipitation and melt in two of the better performing models indicate that use of maximum seasonal air temperatures is not appropriate to use as temperature input.

Model A_{ave} was also used for simulating wildfire influences on seasonal streamflow. The wildfire simulations represented observed streamflow very well, with a low RMSE, high r^2 value, and an overall streamflow bias less than 2.0%. However, results from the wildfire simulations were not as good as Model A_{ave} simulations.

REFERENCES

Alley, W. M. 1984. On the Treatment of Evapotranspiration, Soil Moisture Accounting, and Aquifer Recharge in Monthly Water Balance Models. Water Resources Research **20**:1137-1149.

Atkinson, S., R. Woods, and M. Sivapalan. 2002. Climate and landscape controls on water balance model complexity over changing timescales. Water Resources Research **38**:1314-1331.

Barnett, T., J. Adam, and D. Lettenmaier. 2005. Potential impacts of a warming climate on water availability in snow-dominated regions. Nature:303-309.

Beven, K. 1997. TOPMODEL: A critique. Hydrological Processes **11**:1069-1085.

Beyers, J. L., J. K. Brown, M. D. Busse, L. F. DeBano, W. J. Elliot, P. F. Ffolliott, G. R. Jacoby, J. D. Kneopp, J. D. Landsberg, D. G. Neary, J. R. Reardon, J. N. Rinne, P. R. Robichaud, K. C. Ryan, A. R. Tiedemann, and M. J. Zwolinkski. 2005. Wildland fire in ecosystems: effects of fire on soils and water. . General Technical Report. RMRS-GTR-42-vol.4., U.S. Department of Agriculture, Forest Service,Rocky Mountain Research Station., Ogden, UT.

Biondi, F. 1999. Comparing tree-ring chronologies and repeated timber inventories as forest monitoring tools. Ecological Applications **9**:216-227.

Biondi, F., P. Hartsough, and I. Estrada. 2005. Daily weather and tree growth at the tropical treeline of North America. Arctic Antarctic and Alpine Research **37**:16-24.

Boyle, D., H. Gupta, and S. Sorooshian. 2000. Toward improved calibration of hydrologic models: Combining the strengths of manual and automatic methods. Water Resources Research **16**:3663-3674.

Briffa, K. R., F. H. Schweingruber, P. D. Jones, T. J. Osborn, S. G. Shiyatov, and E. A. Vaganov. 1998. Reduced sensitivity of recent tree-growth to temperature at high northern latitudes. Nature **391**:678-682.

Brockerhoff, M. P. 2000. An Urbanizing World. Population Bulletin **55**:1.

Bunn, A. G., L. J. Graumlich, and D. L. Urban. 2005. Trends in twentieth-century tree growth at high elevations in the Sierra Nevada and White Mountains, USA. Holocene **15**:481-488.

Butts, M. B., J. T. Payne, M. Kristensen, and H. Madsen. 2004. An evaluation of the impact of model structure on hydrological modelling uncertainty for streamflow simulation. Journal of Hydrology **298**:242-266.

Campelo, F., C. Nabais, I. García-González, P. Cherubini, E. Gutiérrez, and H. Freitas. 2009. Dendrochronology of Quercus ilex L. and its potential use for climate reconstruction in the Mediterranean region. Canadian Journal of Forest Research **39**:2486-2493.

Clow, D. W. 2010. Changes in the Timing of Snowmelt and Streamflow in Colorado: A Response to Recent Warming. Journal of Climate:2293-2306.

Daly, C., R. Neilson, and D. Phillips. 1994. A Statistical Topography Model for Mapping Climatological Precipitation over Mountainous Terrain. Journal of Applied Meteorology:140-158.

Day, C. A. 2009. Modelling impacts of climate change on snowmelt runoff generation and streamflow across western U.S. mountain basins: A review of techniques and applications for water resource management. Progress in Physical Geography **33**:614-633.

Farmer, D., M. Sivapalan, and C. Jothityangkoon. 2003. Climate, soil, and vegetation controls upon the variability of water balance in temperate and semiarid landscapes: Downward approach to water balance analysis. Water Resources Research:-.

Ferguson, R. R. 1999. Snowmelt runoff models. Progress in Physical Geography **23**:205-227.

Field, C. B., L. D. Mortsch, M. Brklacich, D. L. Forbes, P. Kovacs, J. A. Patz, S. W. Running, and M. J. Scott. 2007. North America. Climate Change 2007: Impacts, Adaptation and Vulnerability. *Contribution of Working Group II to the Fourth Assessment Report of the Intergovernmental Panel on Climate Change*. U.S. G.P.O. : For sale by the Supt. of Docs., U.S. G.P.O., Washington.

Fiering, M. B. 1967. Streamflow synthesis. Harvard University Press, Cambridge,.

Gray, S. T., and G. J. McCabe. 2010. A combined water balance and tree ring approach to understanding the potential hydrologic effects of climate change in the central Rocky Mountain region. Water Resources Research **46**:W05513.

Grayson, D. K. 1993. The Desert's Past: A Natural Prehistory of the Great Basin. Smithsonian Institution Press, Washington D.C.

Hidalgo, H. G., T. Das, M. D. Dettinger, D. R. Cayan, D. W. Pierce, T. P. Barnett, G. Bala, A. Mirin, A. W. Wood, C. Bonfils, B. D. Santer, and T. Nozawa. 2009. Detection and Attribution of Streamflow Timing Changes to Climate Change in the Western United States. Journal of Climate **22**:3838-3855.

Hill, M. 1975. Geology of the Sierra Nevada. University of California Press, Berkeley.

Hock, R. 2003. Temperature index melt modelling in mountain areas. Journal of Hydrology **282**:104-115.

Hornberger, G. M. 1998. Elements of physical hydrology. Johns Hopkins University Press, Baltimore.

Horton, G. A. 1996. Walker River chronology : a chronological history of the Walker River and related water issues. 1996, 4th update. edition. Nevada Division of Water Planning, Dept. of Conservation and Natural Resources, Carson City, Nev.

Hundley, N. 1992. The great thirst : Californians and water, 1770s-1990s. University of California Press, Berkeley.

Hurteau, M., J. Zald, and M. North. 2007. Species-specific response to climate reconstruction in upper-elevation mixed-conifer forests of the western Sierra Nevada, California. Canadian Journal of Forest Research **37**:1681-1691.

Jones, D. W. 1999. Reference Evapotranspiration. California Irrigation Management Information System. www.cimis.water.ca.gov/cimis/images/etomap.jpg; accessed October 2009.

Kelleners, T. J., D. G. Chandler, J. P. McNamara, M. M. Gribb, and M. S. Seyfried. 2010. Modeling Runoff Generation on in a Small Snow-Dominated Mountainous Catchment. Vadose Zone Journal **9**:517-527.

Krammes, J. S., and L. F. DeBano. 1965. Soil Wettability: A Neglected Factor in Water Managment. Water Resources Research **1**:4.

Maidment, D. R. 1993. Handbook of hydrology. McGraw-Hill, New York.

Marks, D., J. Domingo, D. Susong, T. Link, and D. Garen. 1999. A spatially distributed energy balance snowmelt model for application in mountain basins. **13**:1935 - 1959.

Maurer, E., I. Stewart, C. Bonfils, P. Duffy, and D. Cayan. 2007. Detection, attribution, and sensitivity of trends toward earlier streamflow in the Sierra Nevada. Journal of Geophysical Research-Atmospheres **112**.

Maurer, E. P. 2007. Uncertainty in hydrologic impacts of climate change in the Sierra Nevada, California, under two emissions scenarios. Climatic Change:309-325.

Maxime, C., and D. Hendrik. 2011. Effects of climate on diameter growth of co-occurring Fagus sylvatica and Abies alba along an altitudinal gradient. Trees-Structure and Function **25**:265-276.

McCabe, G. J., and S. L. Markstrom. 2007. A Monthly Water-Balance Model Driven By a Graphical User Interface.

Natural Resources Conservation Service (NRCS). 1993. National Engineering Handbook. USDA-NRCS, Engineering Division. U.S. Gov. Print. Office, Washington, DC. Part 630, Section 4, Chapter 7.

Neary, D. G., G. J. Gottfried, L. F. DeBano, and A. Tecle. 2003. Impacts of Fire on Watershed Resources. Journal of the Arizona-Nevada Academy of Science **35**:23-41.

Nevada Division of Wildlife (NDOW). 2010. Mason Valley Wildlife Management Area. www.ndow.org/about/pubs/wma/wma_mason.pdf; accessed June 2010.

NVenergy. 2010. Where our power comes from. www.nvenergy.com/company/energytopics/where.cfm; accessed June 2010.

Osborn, J. F., R. E. Pelishek, J. S. Krammes, and J. Letey. 1964. Soil Wettability as a factor in erodibility. Pages 294-295 *in* Soil Science Society of America Proceedings.

Oudin, L., C. Perrin, T. Mathevet, V. Andréassian, and C. Michel. 2006. Impact of biased and randomly corrupted inputs on the efficiency and the parameters of watershed models. Journal of Hydrology **320**:62-83.

Ponce, V. M., and A. V. Shetty. 1995. A conceptual model of catchment water balance: 2. Application to runoff and baseflow modeling. Journal of Hydrology **173**:41-50.

Rau, B. M., J. C. Chambers, R. R. Blank, and W. W. Miller. 2005. Hydrologic Response of a Central Nevada Pinyon-Juniper Woodland to Prescribed Fire. Rangeland Ecology & Management **58**:614-622.

Reed, R. D. 1933. Geology of California. American Association of Petroleum Geologists, Tulsa, OK.

Saito, L., F. Biondi, J. D. Salas, A. K. Panorska, and T. J. Kozubowski. 2008. A watershed modeling approach to streamflow reconstruction from tree-ring records. Environmental Research Letters **3**.

Salas, J. D., and A. Cardenas. 1989. SEAMOD, Seasonal Model for Watershed Simulation. Colorado State University, Fort Collins, CO.

Scott, D. F., and D. B. Van Wyk. 1990. The effects of wildfire on soil wettability and hydrological behaviour of an afforested catchment. Journal of Hydrology **121**:239-256.

Seager, R., M. Ting, I. Held, Y. Kushnir, J. Lu, G. Vecchi, H. Huang, N. Harnik, A. Leetmaa, N. Lau, C. Li, J. Velez, and N. Naik. 2007. Model projections of an imminent transition to a more arid climate in southwestern North America. Science **316**:1181-1184.

Sharpe, S. E., M. E. Cablk, J. M. Thomas, and Nevada System of Higher Education. Desert Research Institute. 2007. The Walker Basin, Nevada and California : physical environment, hydrology, and biology. Desert Research Institute, [Reno, Nev.

Sheppard, P. R. 2010. Dendroclimatology: extracting climate from trees. Wiley Interdisciplinary Reviews: Climate Change **1**:343-352.

Shevenell, L. A. 1996. Statewide potential evapotranspiration maps for Nevada. University of Nevada, Reno. Mackay School of Mines. Reno, NV.

Solander, K., L. Saito, and F. Biondi. 2010. Streamflow simulation using a water-balance model with annually-resolved inputs. Journal of Hydrology **387**:46-53.

Stanzel, P., U. Haberl, and H. P. Nachtnebel. 2008. Modelling snow accumulation and snow melt in a continuous hydrological model for real-time flood forecasting. Page 012016. IOP Publishing Ltd., Place of Publication: Bled, Slovenia. Country of Publication: UK.

Stewart, I. T., D. R. Cayan, and M. D. Dettinger. 2004. Changes in snowmelt runoff timing in western North America under a 'business as usual' climate change scenario. Climatic Change:217-232.

Stewart, I. T., D. R. Cayan, and M. D. Dettinger. 2005. Changes toward Earlier Streamflow Timing across Western North America. Journal of Climate **18**:1136-1155.

Swetnam, T. W., C. D. Allen, and J. L. Betancourt. 1999. Applied historical ecology: Using the past to manage for the future. Ecological Applications **9**:1189-1206.

Thornthwaite, C. W. 1948. An Approach toward a Rational Classification of Climate. Geographical Review **38**:55-94.

U.S. Geological Survey (USGS). 2010. Hydrology of the Walker River Basin. U.S. Department of Interior.

Vogel, R.M. 2006. Regional Calibration of Watershed Models. *In* Singh, V.P., Frevert, D.K (eds.) Watershed Models, New York: Taylor & Francis, 653 p.

Wagener, T., N. McIntyre, M. J. Lees, H. S. Wheater, and H. V. Gupta. 2003. Towards reduced uncertainty in conceptual rainfall-runoff modelling: dynamic identifiability analysis. Hydrological Processes **17**:476.

Wagener, T., and H. S. Wheater. 2006. Parameter estimation and regionalization for continuous rainfall-runoff models including uncertainty. Journal of Hydrology **320**:132-154.

Walter, M. T., E. S. Brooks, D. K. McCool, L. G. King, M. Molnau, and J. Boll. 2005. Process-based snowmelt modeling: does it require more input data than temperature-index modeling? Journal of Hydrology **300**:65-75.

Westerling, A. L., H. G. Hidalgo, D. R. Cayan, and T. W. Swetnam. 2006. Warming and Earlier Spring Increase Western U.S. Forest Wildfire Activity. Science **313**:940-943.

Western Regional Climate Center (WRCC). 2006. Desert Research Institute. Reno, NV.

Wilkinson, C. F. 1992. Crossing the next meridian : land, water, and the future of the West. Island Press, Washington, D.C.

Wohlegemuth, P. M., K. Hubbert, and M. J. Arbaugh. 2006. Fire and physical environment interactions: soil, water, and air. University of California Press, Berkeley, CA.

Woodhouse, C. A. 2003. A 431-Yr Reconstruction of Western Colorado Snowpack from Tree Rings. Journal of Climate **16**:1551.

Woodhouse, C. A., J. L. Russell, and E. R. Cook. 2009. Two Modes of North American Drought from Instrumental and Paleoclimatic Data. Journal of Climate **22**:4336-4347.

Xu, C. Y. 2002. Mathematical models of small watershed hydrology and applications. Water Resources Publications, Highlands Ranch, CO.

Xu, C. Y., and V. P. Singh. 1998. A Review on Monthly Water Balance Models for Water Resources Investigations. Water Resources Management **12**:20-50.

Yates, D. N. 1996. WatBal: An Integrated Water Balance Model for Climate Impact Assessment of River Basin Runoff. International Journal of Water Resources Development **12**:121-140.

Young, C. A., M. I. Escobar-Arias, M. Fernandes, B. Joyce, M. Kiparsky, J. F. Mount, V. K. Mehta, D. Purkey, J. H. Viers, and D. Yates. 2009. Modeling the Hydrology of Climate Change in California's Sierra Nevada for Subwatershed Scale Adaptation1. Journal of the American Water Resources Association **45**:1409-1423.

APPENDIX

Initial parameter values were investigated for the best performing model, Model A_{ave} (Model A using average seasonal temperatures) and the corresponding Model B, Model B_{ave}, over parameter space to better evaluate the influences of individual parameters on each performance metric for RMSE, r^2, and overall %bias (Figures 18-29). Initial values generated during the Monte Carlo-styled approach varied within parameter space set by model boundary condition constraints, with all parameters covering parameter space with an even distribution based upon constraints. The upper boundary condition was set at 0.9 for parameter *a* (runoff fraction) as in Saito et al. (2008) based on Soil Group D (NRCS 1993). The upper boundary condition for *b* (ET fraction), *c* (baseflow fraction), and *d* (groundwater flow fraction) was set to 1.0, as ET, baseflow, and GW flow could not exceed available infiltrated water or GW storage (Saito et al. 2008). Lower boundary conditions for *a*, *b*, *c*, and *d* were set to 0.0. Boundary conditions for the snow component in the models, *s*, *w*, *e*, *f*, and *m*, were based on Solander et al. (2010) and Gray and McCabe (2010), and ranged between 0.0 ^{o}C to 3.89 ^{o}C, with parameter *s* and *e* always being greater than *w* and *f*, respectively. In order to prevent temperature parameters from being identical, which prevented the model from running, a constraint was added to require a 0.2 ^{o}C difference in temperature between parameters *s* and *w* for Model A_{ave}, and between parameters *e* and *f* for Model B_{ave}, which was determined to be the minimum temperature difference necessary based on model functionality.

As parameter *a* values approach 0.6, RMSE is minimized, while %bias is consistently reduced as parameter *a* values increase. r^2 values also seem to be higher when parameter *a* increases, with the range of values narrowing after the value of *a* reaches about 0.5. Parameters *b,* and *d* do not appear to influence r^2, however, all parameters at all values do not improve r^2 above a threshold of 0.91. RMSE remains consistent over parameter space for parameter *b* and %bias consistently decreased as parameter value increased, consistent with an under-estimation of streamflow due to a greater fraction of water lost to ET. Parameters *c* and *d* show a similar RMSE trend of remaining consistent across parameter space, with RMSE becoming slightly more variable at higher parameter values. Snow parameters for Model A_{ave} seem to indicate that parameter *s* (temperature below which all precipitation is snow) influences r^2, but not %bias or RMSE. When temperature ranges between 0.0 ^oC and around 0.75 ^oC, r^2 increases as temperature increases, however, when temperature reaches around 0.75 ^oC, r^2 does not improve until temperature reaches around 1.0 ^oC. After 1.0 ^oC, r^2 does not increase beyond 0.91. Parameter *w* (temperature above which snowmelt begins) appears to influence r^2 at lower temperatures.

Model B_{ave} appears not to be as strongly influenced by parameter *a*, with RMSE remaining relatively constant across parameter space. Around parameter value 0.6, RMSE appears to increase slightly as parameter values increase. RMSE remained relatively constant across parameter space for parameters *b*, *c*, and *d*, and r^2 did not appear to be influenced by parameters *a*, *b*, *c*, or *d*, with r^2 remaining constant over parameter space as well. When %bias was investigated, it appears that parameter *a*

strongly controlled estimation of streamflow, with %bias indicating under-estimation of streamflow until parameter values reached around 0.2, after which %bias increased greatly and became more varied. Parameters *b*, *c*, and *d* did not appear to influence %bias in Model B_{ave}. Assessment of parameter *m*, meltmax, appears to indicate that as values of *m* increase RMSE and % bias variability increase, while variability in r^2 sharply decreases at values around 0.3, with r^2 values ranging between 0.0 and 0.2.

Figure 18: Model A_{ave} initial *a*, *b*, *c* and *d* parameter values over 500 runs plotted against RMSE.

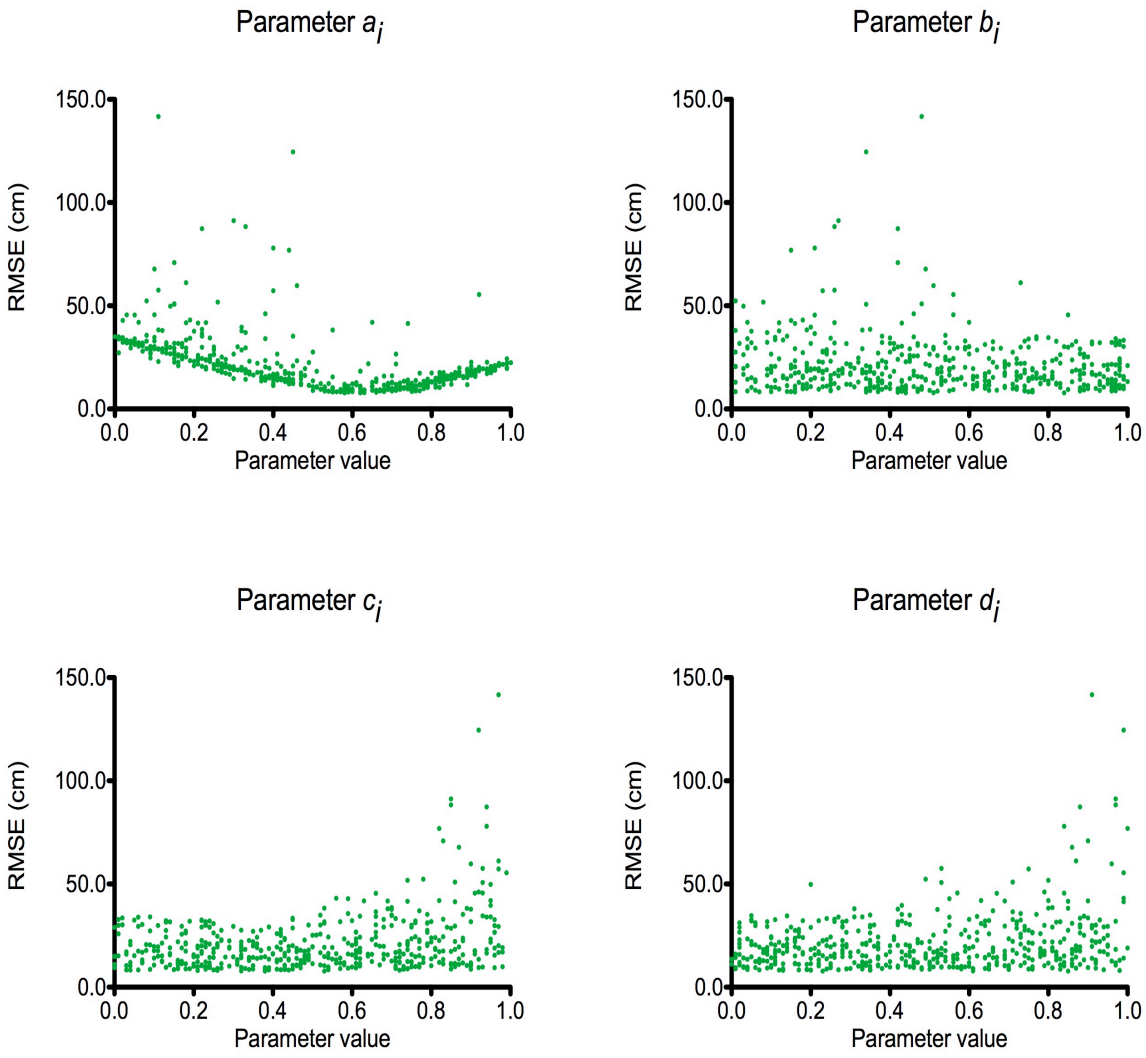

Figure 19: Model A_{ave} initial *s* and *w* parameter values over 500 runs plotted against RMSE.

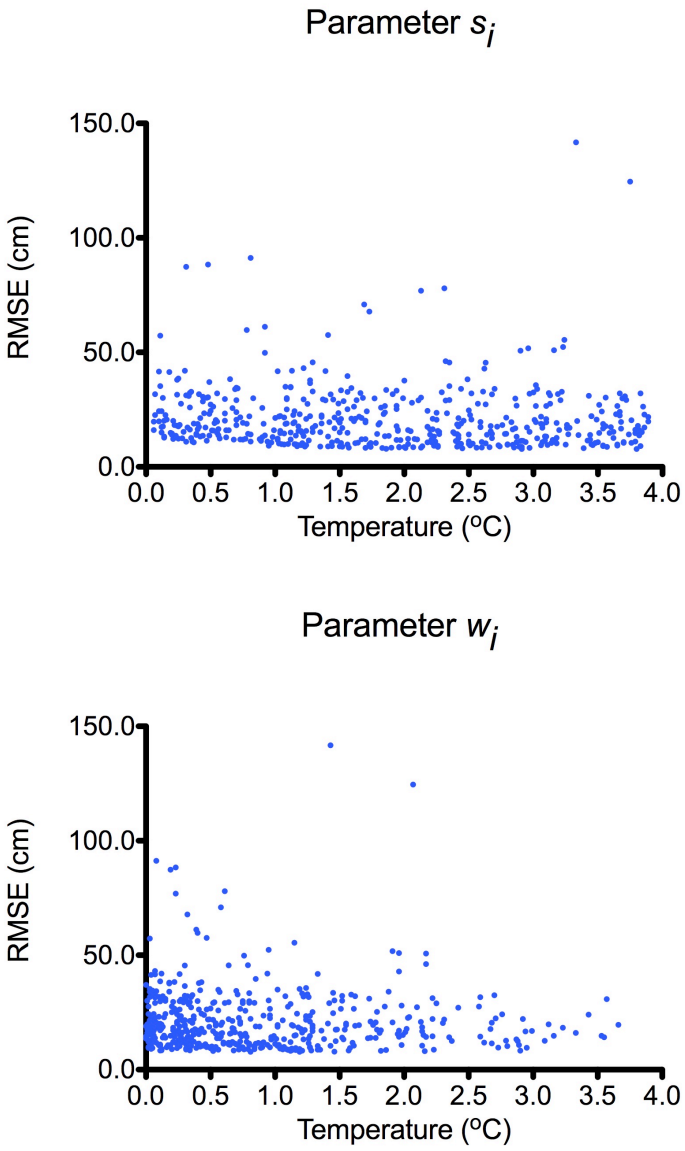

Figure 20: Model B_{ave} initial *a*, *b*, *c* and *d* parameter values over 500 runs plotted against RMSE.

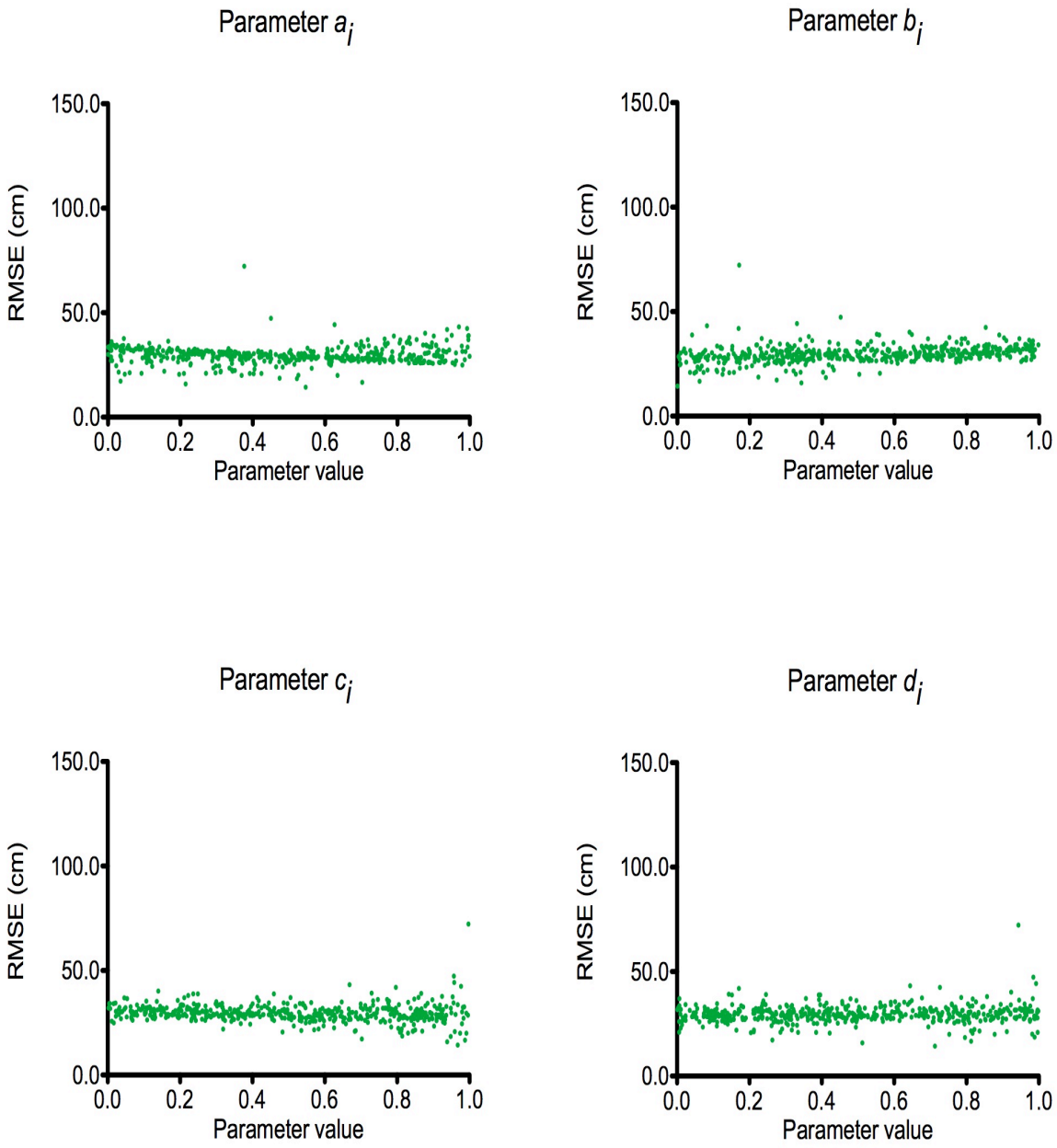

Figure 21: Model B_{ave} initial *e, f* and *m* parameter values over 500 runs plotted against RMSE.

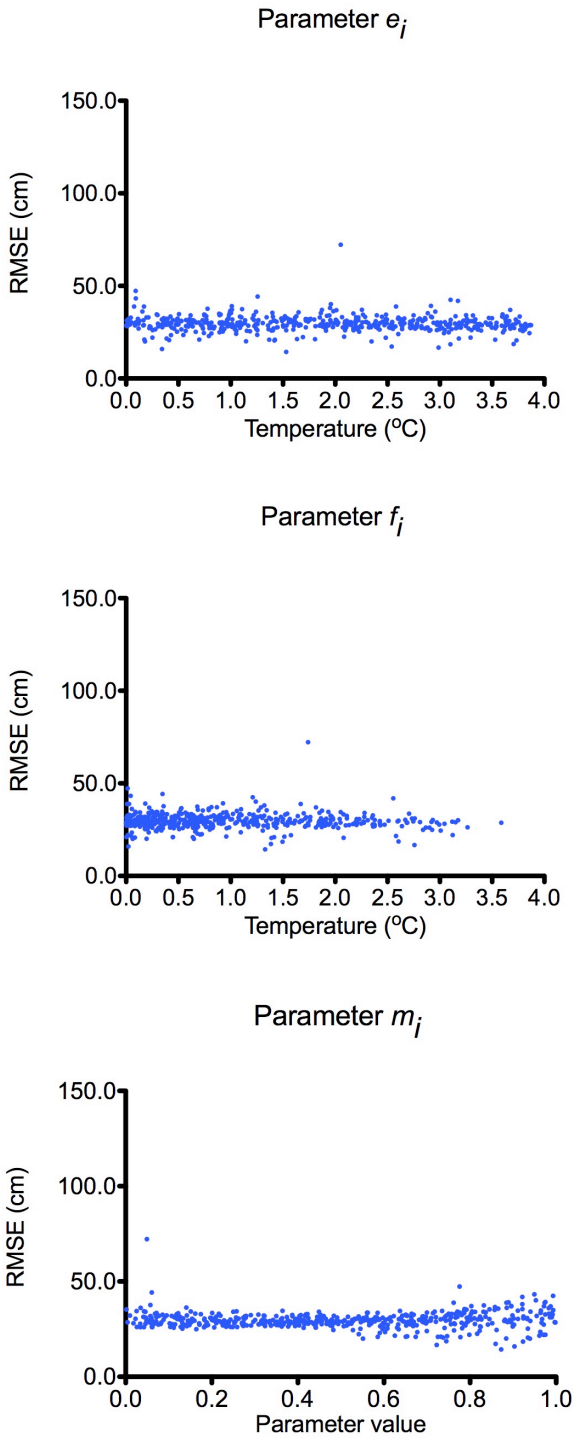

Figure 22: Model A_{ave} initial *a*, *b*, *c* and *d* parameter values over 500 runs plotted against r^2.

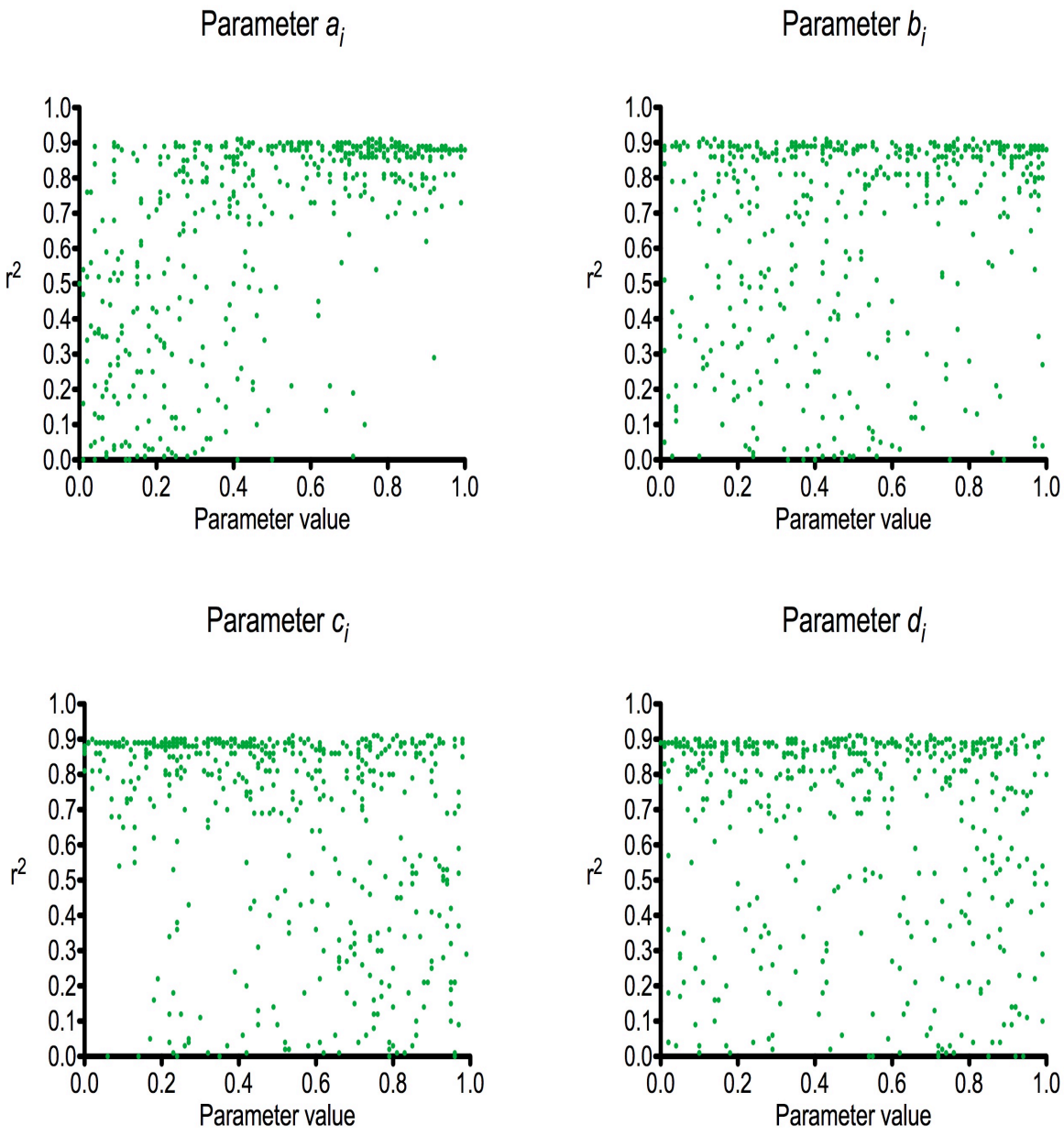

Figure 23: Model A_{ave} initial *s* and *w* parameter values over 500 runs plotted against r^2.

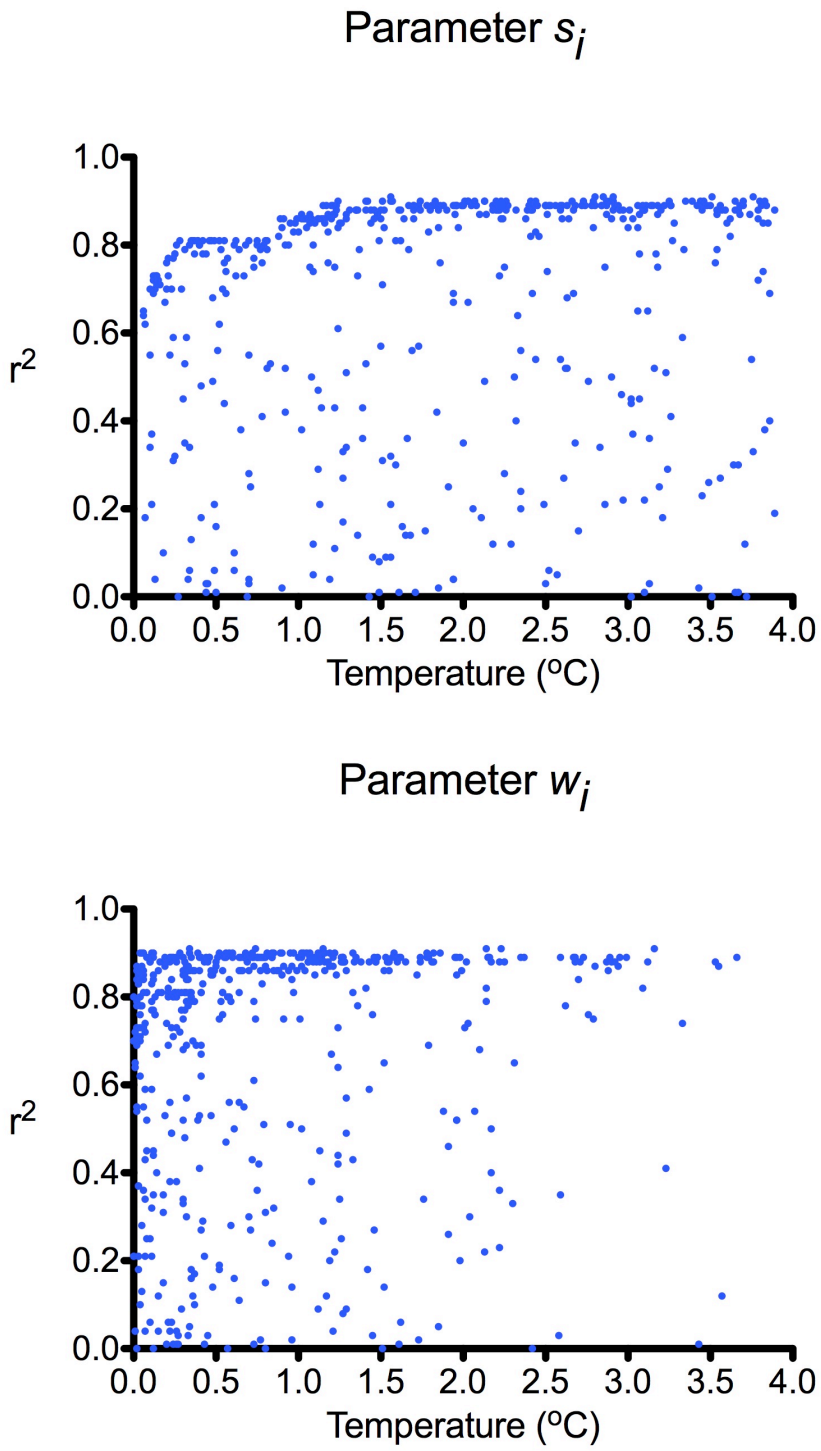

Figure 24: Model B_{ave} initial *a*, *b*, *c* and *d* parameter values over 500 runs plotted against r^2.

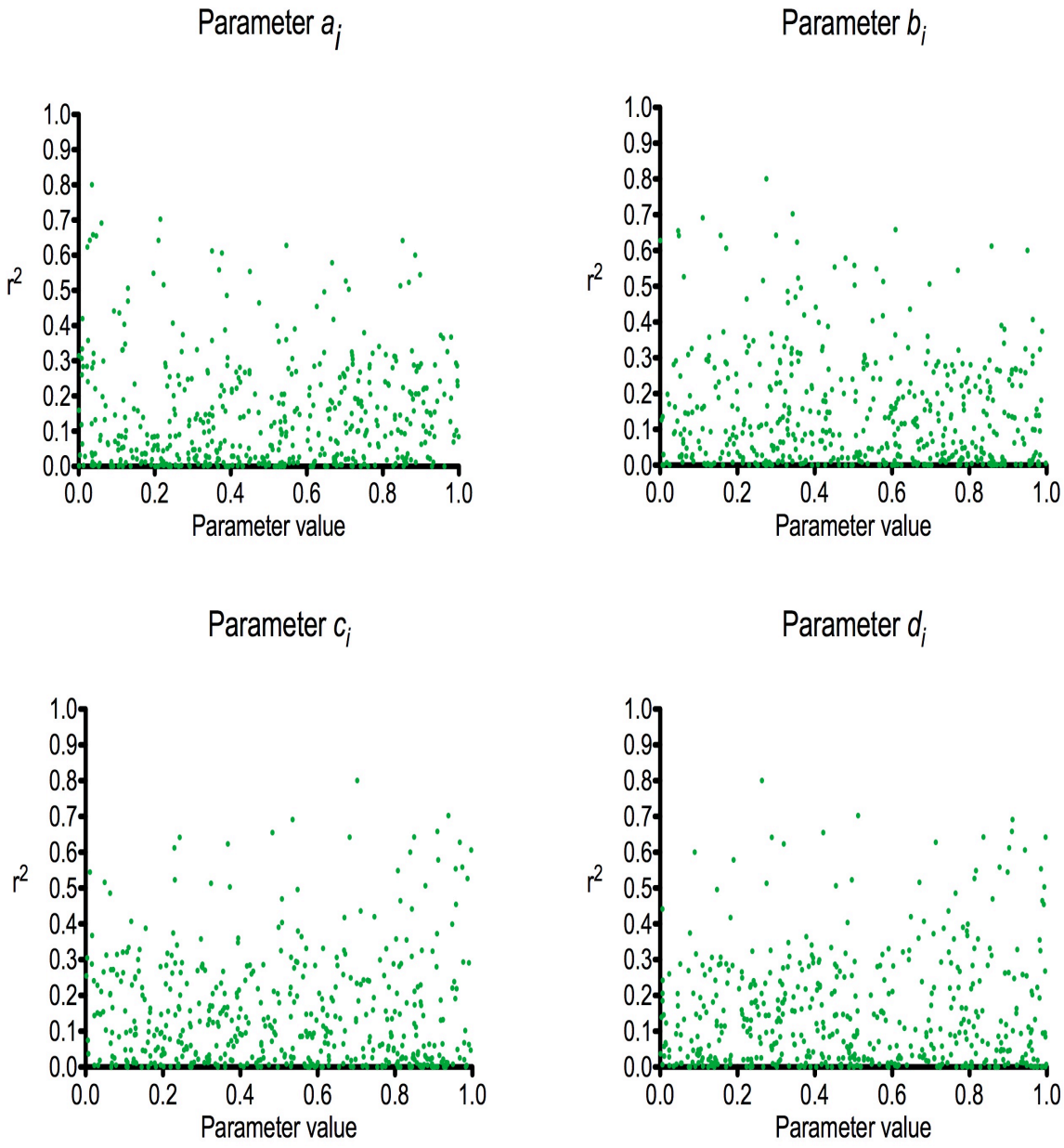

Figure 25: Model B_{ave} initial *e*, *f* and *w* parameter values over 500 runs plotted against r^2.

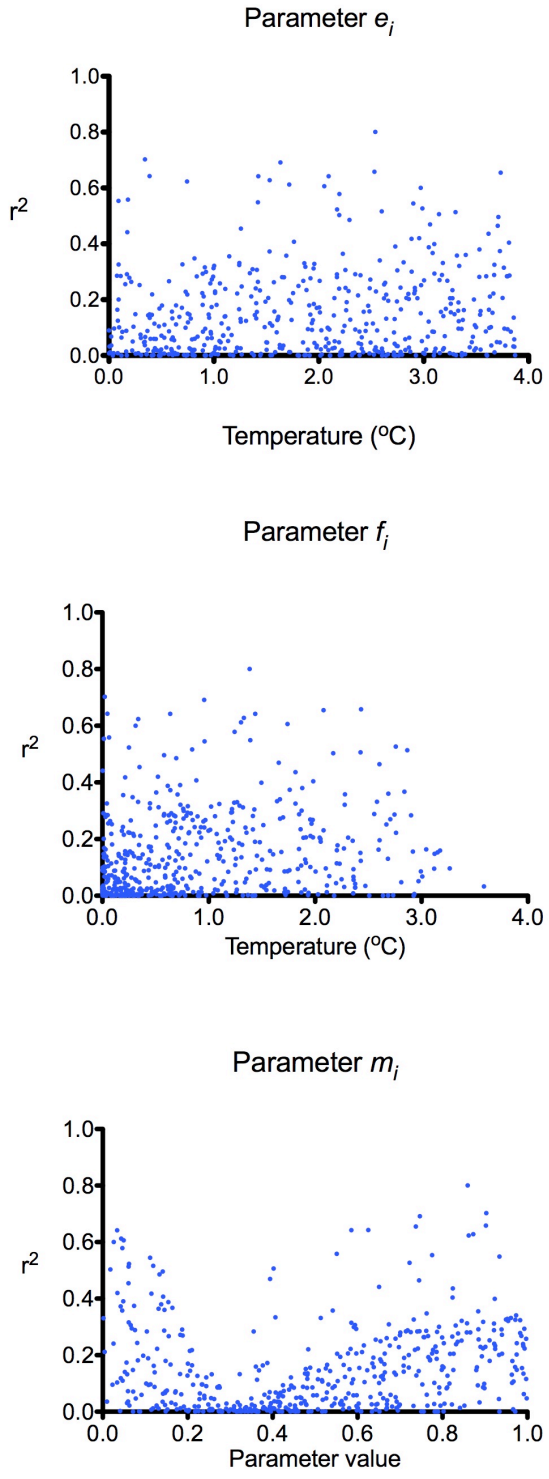

Figure 26: Model A_{ave} initial *a*, *b*, *c* and *d* parameter values over 500 runs plotted against %bias.

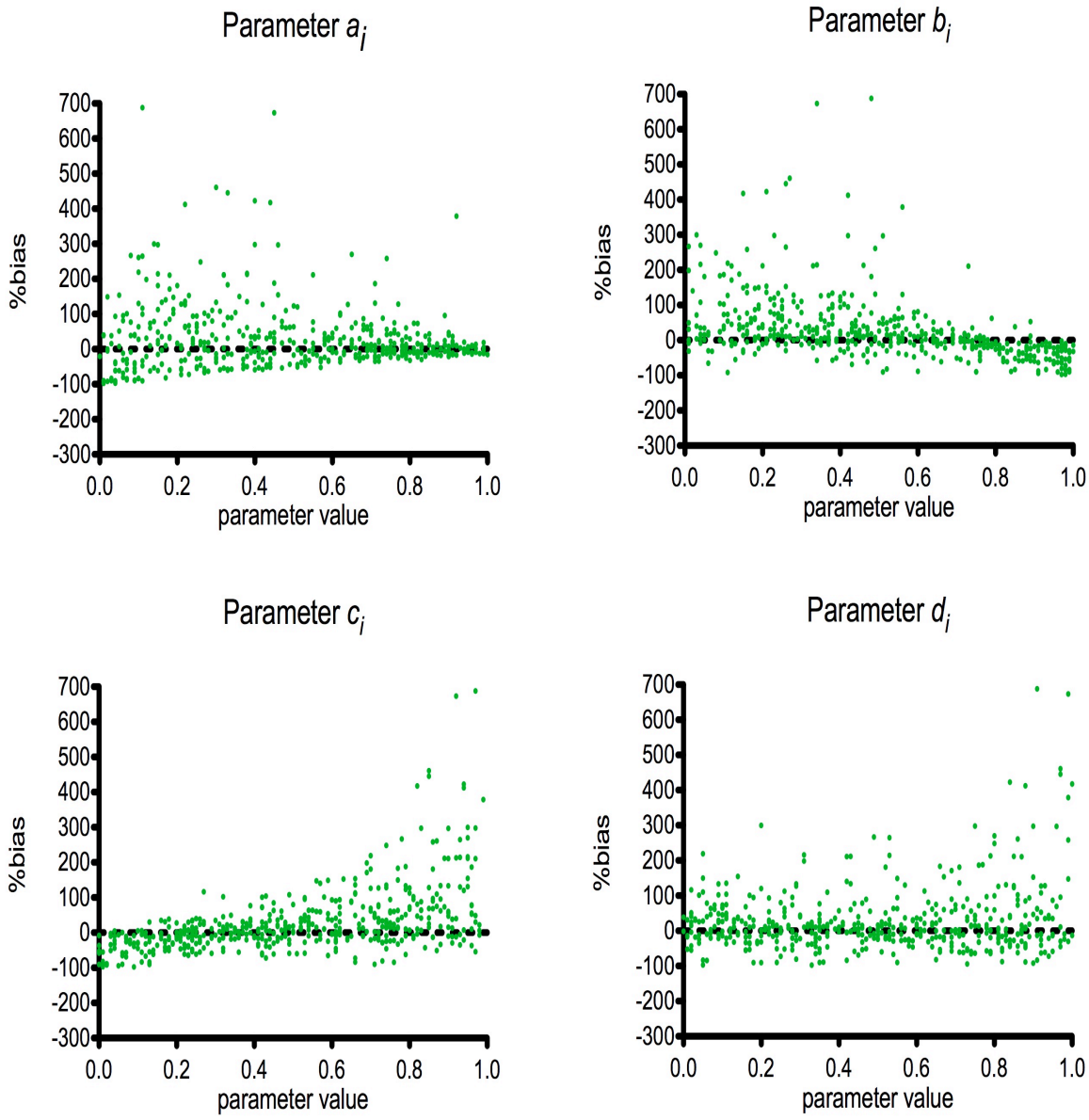

Figure 27: Model A_{ave} initial *s* and *w* parameter values over 500 runs plotted against %bias.

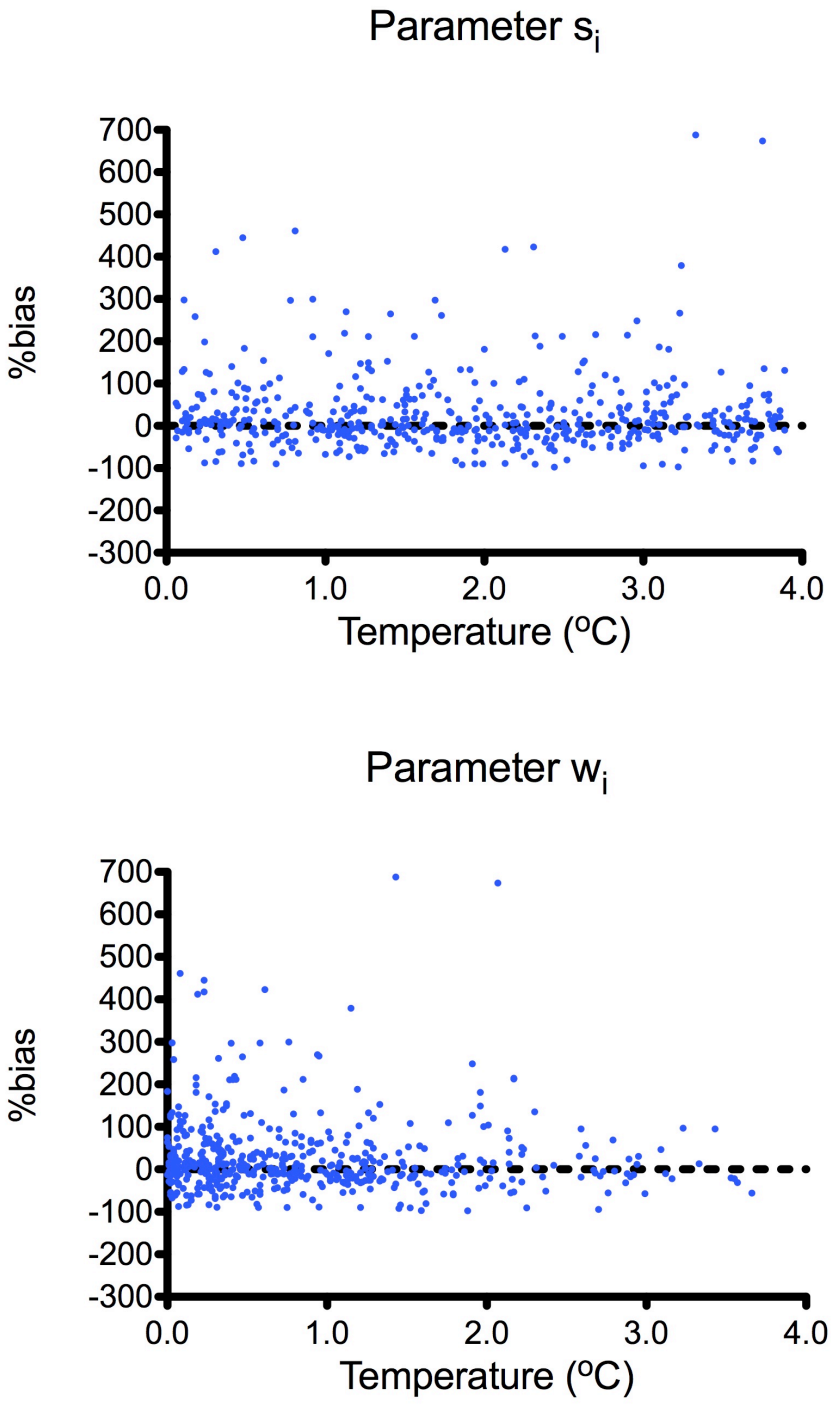

Figure 28: Model B_{ave} initial *a*, *b*, *c* and *d* parameter values over 500 runs plotted against %bias.

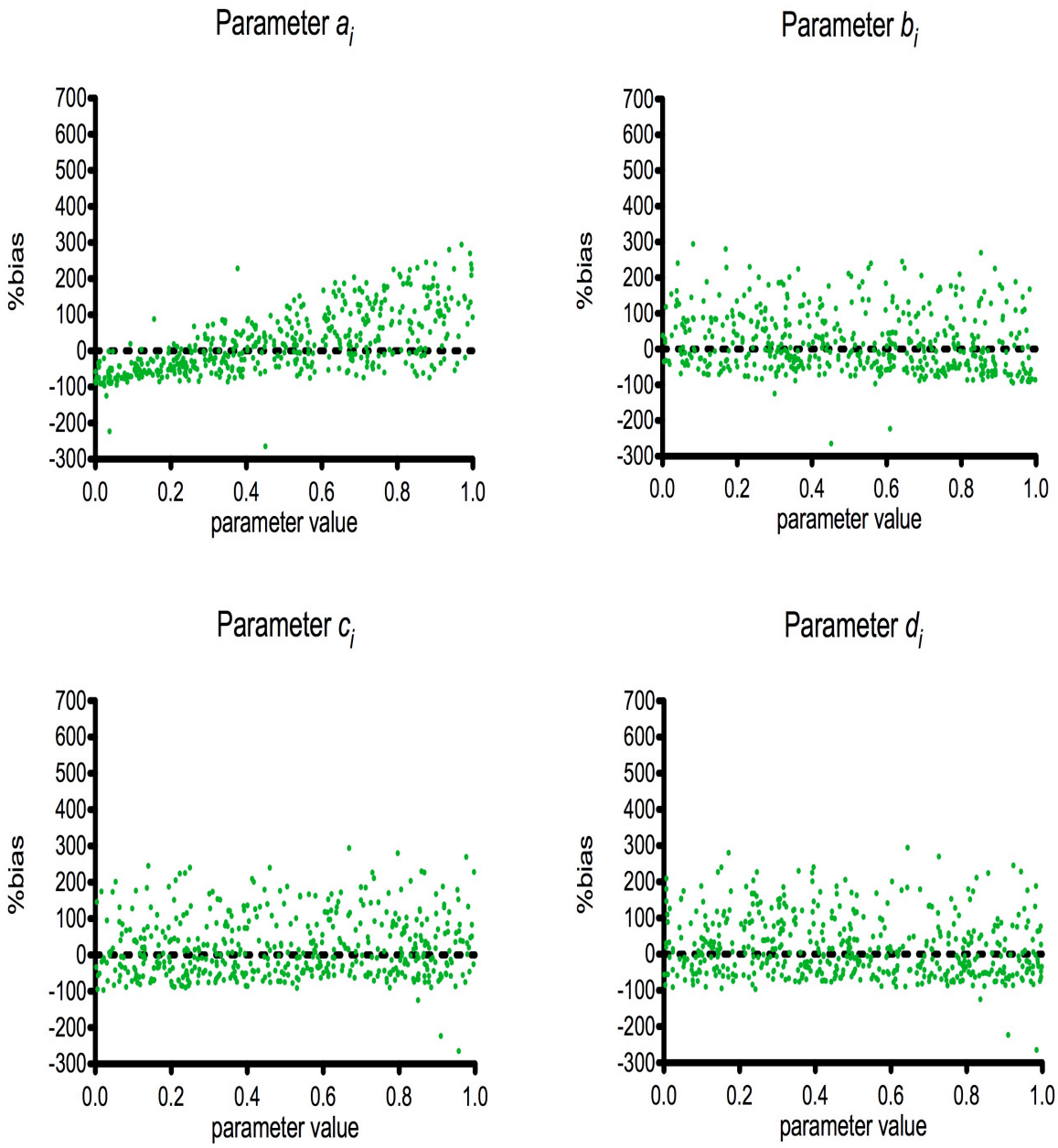

Figure 29: Model B_{ave} initial *e*, *f* and *m* parameter values over 500 runs plotted against %bias.